

WL-TR-95-4080



LAYERED CERAMIC COMPOSITE BEARINGS WITH
IMPROVED DAMAGE RESISTANCE AND RELIABILITY

R A CUTLER OF CERAMATEC, INC
D K SHETTY, L Y CHAO AND R LAKSHMINARAY
OF UNIVERSITY OF UTAH

CERAMATEC, INC
2425 SOUTH 900 WEST
SALT LAKE CITY, UTAH 84119

AUGUST 1994

FINAL REPORT FOR 04/01/92-06/01/94

APPROVED FOR PUBLIC RELEASE; DISTRIBUTION IS UNLIMITED.

19960415 097

MATERIALS DIRECTORATE
WRIGHT LABORATORY
AIR FORCE MATERIEL COMMAND
WRIGHT PATTERSON AFB OH 45433-7734

DTIC QUALITY INSPECTED 1

NOTICE

When government drawings, specifications, or other data are used for any purpose other than in connection with a definitely related government procurement operation, the United States Government thereby incurs no responsibility nor any obligation whatsoever; and the fact that the government may have formulated, furnished, or in any way supplied the said drawings, specifications, or other data, is not to be regarded by implication or otherwise as in any manner licensing the holder or any other person or corporation, or conveying any rights or permission to manufacture, use, or sell any patented invention that may in any way be related thereto.

This report is releasable to the National Technical Information Service (NTIS). At NTIS, it will be available to the general public, including foreign nations.

This technical report has been reviewed and is approved for publication.

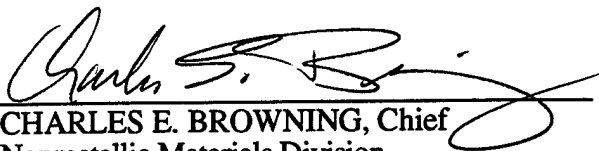


KARL R. MECKLENBURG, Project Engineer
Nonstructural Materials Branch
Nonmetallic Materials Division



KENT J. EISENTRAUT, Chief
Nonstructural Materials Branch
Nonmetallic Materials Division

FOR THE COMMANDER



CHARLES E. BROWNING, Chief
Nonmetallic Materials Division
Materials Directorate

If your address has changed, if you wish to be removed from our mailing list, or if the addressee is no longer employed by your organization, please notify WL/MLBT, Bldg 654, 2941 P Street, Suite 1, Wright-Patterson AFB OH 45433-7750 to help maintain a current mailing list.

Copies of this report should not be returned unless return is required by security considerations, contractual obligations, or notice on a specific document.

REPORT DOCUMENTATION PAGE			Form Approved OMB No. 0704-0188	
Public reporting burden for this collection of information is estimated to average 1 hour per response, including the time for reviewing instructions, searching existing data sources, gathering and maintaining the data needed, and completing and reviewing the collection of information. Send comments regarding this burden estimate or any other aspect of this collection of information, including suggestions for reducing this burden, to Washington Headquarters Services, Directorate for Information Operations and Reports, 1215 Jefferson Davis Highway, Suite 1204, Arlington, VA 22202-4302, and to the Office of Management and Budget, Paperwork Reduction Project (0704-0188), Washington, DC 20503.				
1. AGENCY USE ONLY (Leave blank)	2. REPORT DATE AUG 1994	3. REPORT TYPE AND DATES COVERED FINAL 04/01/92--06/01/94		
4. TITLE AND SUBTITLE LAYERED CERAMIC COMPOSITE BEARINGS WITH IMPROVED DAMAGE RESISTANCE AND RELIABILITY		5. FUNDING NUMBERS C F33615-92-C-5915 PE 62712 PR 8355 TA 00 WU 11		
6. AUTHOR(S) A CUTLER OF CERAMATEC, INC D K SHETTY, L Y CHAO AND R LAKSHMINARAY OF UNIVERSITY OF UTAH				
7. PERFORMING ORGANIZATION NAME(S) AND ADDRESS(ES) CERAMATEC, INC 2425 SOUTH 900 WEST SALT LAKE CITY, UTAH 84119		8. PERFORMING ORGANIZATION REPORT NUMBER 9469306		
9. SPONSORING/MONITORING AGENCY NAME(S) AND ADDRESS(ES) MATERIALS DIRECTORATE WRIGHT LABORATORY AIR FORCE MATERIEL COMMAND WRIGHT PATTERSON AFB OH 45433-7734		10. SPONSORING/MONITORING AGENCY REPORT NUMBER WL-TR-95-4080		
11. SUPPLEMENTARY NOTES				
12a. DISTRIBUTION/AVAILABILITY STATEMENT APPROVED FOR PUBLIC RELEASE; DISTRIBUTION IS UNLIMITED.		12b. DISTRIBUTION CODE		
<p>13. ABSTRACT Hybrid bearings incorporating hot-isostatically-pressed (HIPed) silicon nitride elements (balls and rollers) have demonstrated excellent performance in a variety of applications. The single-most important factor limiting the greater use of silicon nitride elements is cost. One method for reducing cost is to develop alternate ceramic bearing elements that can deliver the performance of silicon nitride but at significantly reduced costs. It was hypothesized that by putting the surface of bearings under strong residual compression the price could be reduced and the reliability of the materials could be improved.</p> <p>Layered ceramic rods with residual surface compression from thermal-expansion mismatch of the coating with the substrate were made by either slip casting and cosintering or chemical vapor deposition (CVD) coating sintered substrates. CVD SiC deposited on SiC-30 vol. % TiC resulted in high compression (680 MPa) in the outer layer of two-layer rods. The fatigue lifetimes at a failure probability of 0.5 increased from ≈ 1.5 million stress cycles for CVD SiC with ≈ 140 MPa surface compression to over 50 million cycles for the same CVD SiC with ≈ 680 MPa compression. The enhanced fatigue lifetime of SiC with high surface compression was accompanied by improved wear resistance, showing that SiC is a candidate bearing material when it has high apparent toughness and low porosity. Defects in the CVD coating still limited the performance of the bearings. Development of alternate substrates that can be manufactured from inexpensive raw materials, CVD coating in a fluidized bed to limit coating defects, and more economical surface finishing are discussed as means of making lower cost ceramic bearings.</p>				
14. SUBJECT TERMS Ceramic bearings, rolling contact fatigue testing, residual stress, composites		15. NUMBER OF PAGES 59		
		16. PRICE CODE		
17. SECURITY CLASSIFICATION OF REPORT UNCLASSIFIED	18. SECURITY CLASSIFICATION OF THIS PAGE UNCLASSIFIED	19. SECURITY CLASSIFICATION OF ABSTRACT UNCLASSIFIED	20. LIMITATION OF ABSTRACT SAR	

TABLE OF CONTENTS

	Page
1. EXECUTIVE SUMMARY.....	1
2. INTRODUCTION.....	5
2.1 Research Objectives.....	7
2.2 Technical Background.....	7
2.3 Proposed Research.....	14
3. EXPERIMENTAL PROCEDURES	19
4. RESULTS AND DISCUSSION	22
4.1 Materials Selection and Rheology Development.....	22
4.2 Slip Cast and Cosintered Materials.....	28
4.3 CVD Coatings	35
5. TECHNOLOGY TRANSFER/COMMERCIALIZATION PLANS.....	54
6. CONCLUSIONS.....	56
7. ACKNOWLEDGMENTS.....	56
8. REFERENCES	57

List of Figures

<u>Figure</u>	<u>Page</u>
1. Linearized Weibull plots of fracture stresses (four-point bend strength) of monolithic and three-layer zirconia-toughened alumina composites	8
2. Decrease in fracture strengths of slip cast three-layer and monolithic zirconia-toughened alumina ceramics with increasing indentation loads	10
3. Fracture strengths (σ_f) versus inverse cube root of indentation load ($P^{-1/3}$) plots for slip cast three-layer and monolithic ZTA ceramics.....	10
4. Schematic of a two-layer roller bearing consisting of Si_3N_4 outer layer and SiC inner layer.....	12
5. Variation of radial, tangential and axial stresses along a radius in the outer layer and part of the inner layer of a two-layer $\text{Si}_3\text{N}_4/\text{SiC}$ roller bearing.....	12
6. A schematic of the three ball-on-rod rolling contact fatigue test machine	21
7. Composition of three-layer RC2-118B/RC2-120A/RC2-118B (see Table 2) composite as a function of distance from the surface as determined by electron microprobe.....	24
8. Phase equilibria for $\text{SiO}_2\text{-Y}_2\text{O}_3\text{-Al}_2\text{O}_3$ [45] showing liquid formation at the temperature used to sinter compositions shown in Table 2	24
9. Agglomerate size distributions of Si_3N_4 (outer layer) and $\text{Si}_3\text{N}_4\text{-15 vol. \% TiN}$ (inner layer) slips dispersed using 1 wt. % 2-amino-2-methylpropanol[52] in water	26
10. Viscosity comparison of $\text{Si}_3\text{N}_4\text{-6 wt. \% Y}_2\text{O}_3\text{-2 wt. \% Al}_2\text{O}_3$ at 35 vol. % solids with $\text{Si}_3\text{N}_4\text{-20 vol. \% TiN}$ at 32.3 vol. % solids	27
11. Weibull plot for 32 bars of liquid phase sintered SiC.....	30
12. Strain as a function of depth of material removed for monolithic SiC-15 vol. % TiC and three-layer SiC-15 vol. % TiC/SiC-30 vol. % TiC/SiC-15 vol. % TiC.....	30
13. Flexural strength measurements as a function of: (a) indentation load, P, and (b) $P^{-1/3}$. Monolithic outer layer material is SiC-15 vol. % TiC, inner-layer is SiC-30 vol. % TiC, and damage resistant material is the three-layer composite.....	31
14. Variation of radial, tangential, and axial stresses along a radius in the outer layer and part of the inner layer of two-layer SiC-15 vol. % TiC/SiC-30 vol. % TiC rod. (a) $E=492$ GPa, (b) $E=435$ GPa	32
15. Weibull plots for monolithic outer layer SiC-15 vol. % TiC and two-layer SiC-15 vol. % TiC/SiC-30 vol. % TiC rods loaded initially at 5.5 GPa	34
16. Variation of radial, tangential, and axial stresses along a radius in the outer layer and part of the inner layer of two-layer $\text{Si}_3\text{N}_4/\text{Si}_3\text{N}_4\text{-15 vol. \% TiN}$ rod.....	34

List of Figures (cont.)

<u>Figure</u>	<u>Page</u>
17. Weibull plots for monolithic outer layer Si_3N_4 and two-layer $\text{Si}_3\text{N}_4/\text{Si}_3\text{N}_4$ -15 vol. % TiN rods loaded initially at 5.5 GPa	35
18. Microstructure of monolithic Si_3N_4 rods tested in rolling contact fatigue at 5.5 GPa showing spall and fracture initiation site	36
19. Microstructure of monolithic Si_3N_4 (left) and layered Si_3N_4 -15 vol. % TiN (right) rods tested in rolling contact fatigue at 5.5 GPa showing spall and fracture initiation site	37
20. Strain as a function of depth of material removed for monolithic Si_3N_4 and three-layer $\text{Si}_3\text{N}_4/\text{Si}_3\text{N}_4$ -20 vol. % TiN/ Si_3N_4	38
21. Weibull plots for Si_3N_4 coated (<20 μm coating) SiC as compared with ground SiC of the same composition	40
22. Weibull plots for SiC coated ($\approx 60 \mu\text{m}$ coating) and uncoated SiC-15 vol. % TiC with identical surface finish.....	41
23. Surface finish comparison between CVD SiC and a commercial Si_3N_4 bearing material finished to the same specifications by the same vendor	42
24. Strain as a function of depth of material removed for monolithic SiC-15 vol. % TiC, CVD SiC/SiC/CVD SiC, and CVD SiC/SiC-30 vol. % TiC/CVD SiC	43
25. Variation of radial and axial stresses along a radius in the outer layer and part of the inner layer of two-layer CVD SiC/SiC and two-layer CVD SiC/SiC-30 vol. % TiC rod.....	43
26. Weibull plots of rolling-contact fatigue lives for monolithic SiC-15 vol. % TiC (open circles), layered CVD SiC/SiC (open squares) and layered CVD SiC/SiC-30 vol. % TiC (solid squares).....	44
27. Optical micrographs of cross-sections of CVD SiC coated on RCF rods. (a) CVD SiC on SiC substrate, (b) CVD SiC on SiC-30 vol. % TiC substrate.....	45
28. SEM micrographs of polished and etched CVD SiC/SiC. (a) Interface between the SiC substrate and the CVD SiC coating, (b) An interface within the CVD SiC coating caused by process interruption.....	46
29. Comparison of wear tracks on (a) CVD SiC on SiC ($\sigma_R = -141 \text{ MPa}$) after one million cycles and (b) CVD SiC on SiC-30 vol. % TiC ($\sigma_R = -679 \text{ MPa}$) after 51.6 million cycles in rolling contact fatigue at 5.5 GPa.....	48
30. Volume loss as a function of RCF stress cycles. Note that "wear" is not measurable for CVD SiC on SiC-30 vol. % TiC due to higher apparent toughness compared to CVD SiC/SiC system	49

List of Figures (cont.)

<u>Figure</u>	<u>Page</u>
31. Fractography of failed CVD SiC/SiC-30 vol. % TiC.....	50
32. Near surface SEM micrographs of polished and etched CVD SiC/SiC-30 vol. % TiC showing SiC nodule growth in CVD process. (a) Layered substructure in CVD SiC coating, (b) interface between two layers in CVD SiC coating.....	52
33. SEM micrographs of polished and etched CVD SiC/SiC-30 vol. % TiC showing defects in CVD SiC. (a) An interface caused by process interruption, (b) large SiC grains (i.e., columnar growth of micrograin SiC) within the CVD SiC coating	53

List of Tables

<u>Table</u>	<u>Page</u>
1. Time Table for Proposed Research.....	18
2. Si_3N_4 and $\text{Si}_3\text{N}_4\text{-Y}_3\text{Al}_5\text{O}_{12}$ Compositions.....	22
3. Characterization of Si_3N_4 and $\text{Si}_3\text{N}_4\text{-Y}_3\text{Al}_5\text{O}_{12}$ Compositions.....	23
4. Si_3N_4 , $\text{Si}_3\text{N}_4\text{-TiN}$, SiC , and SiC-TiC Compositions.....	25
5. Strength Data for SiC and SiC-TiC Composites.....	29
6. Thickness and Strength of CVD Si_3N_4 Deposited at 1000°C for 10 Hours	38
7. Thickness and Residual Stresses Resulting From CVD Si_3N_4 Deposited at 1000°C for 17 Hours.....	39

1. EXECUTIVE SUMMARY

The objective of this program was the development of improved ceramic bearing materials having residual compression in the contact surface that can enhance rolling contact fatigue performance and result in reduced wear and increased reliability (i.e., less scatter in fatigue life).

Layered ceramic rods were prepared using two approaches: 1) chemical vapor deposition (CVD) of Si_3N_4 or SiC on sintered ceramic substrates, and 2) slip casting of layered ceramics and cosintering. In both cases, residual stresses were controlled by the choice of coefficients of thermal expansion, moduli, Poisson's ratios, and thickness of outer and inner layers.

Strain[1], strength, and indentation/strength measurements were used to measure the residual compressive stresses in the outer layers of three-layer bars. These measurements were compared with calculated stresses assuming a square-wave stress distribution.

Scanning electron microscopy was used to characterize the grain size of crystalline constituents and to investigate the adherence between layers. Rolling contact fatigue (RCF) testing was performed using a three ball-on-rod test[2] where the balls were 12.5 mm diameter roughened steel (AISI 52100) and the rod was a monolithic or layered ceramic diamond finished to a diameter of 9.5 mm. Failure modes and wear were investigated using scanning electron microscopy and surface profilometry.

A substantial effort was directed towards finding a vendor who could deposit a 200-300 μm layer of CVD Si_3N_4 on a variety of Si_3N_4 and SiC -based substrates. Astro Technologies coated Si_3N_4 successfully to thicknesses up to 50 μm but was unable to achieve the desired 250 μm thickness. Ultramet was unable to coat Si_3N_4 which adhered to the substrates. The conclusion of these trials was that the deposition rate of Si_3N_4 is too low to be commercially viable and further CVD efforts were directed at SiC .

Baumgartner tested Norton NC 203 SiC and observed catastrophic failure[3]. Baumgartner, certainly aware of the lower toughness of SiC compared to Si_3N_4 , suggested that it would be intriguing to develop bearings with strong residual compressive surface stress. Du Pont Lanxide applied a CVD SiC coating on pressureless sintered SiC [4] and SiC -30 vol. % TiC rods with coefficients of thermal expansion of $5 \times 10^{-6}/^\circ\text{C}$ and $6 \times 10^{-6}/^\circ\text{C}$, respectively. Both materials were coated simultaneously at 1000°C . The residual compressive stresses in the outer layers of two-layer rods of CVD SiC/SiC and of CVD SiC/SiC -30 vol. % TiC were ≈ 140 MPa and ≈ 680 MPa, respectively. The rods were diamond ground using procedures developed by the bearing industry. This finishing

procedure resulted in a surface finish (R_A) of $\approx 3 \times 10^{-2} \mu\text{m}$ ($1.2 \mu\text{in}$). Ball-on-rod testing (at a maximum contact stress of 5.5 GPa) for the two CVD coated materials in comparison with the monolithic SiC-15 vol. % TiC (which behaves similarly in RCF to the monolithic liquid phase sintered SiC and SiC-30 vol. % TiC) and M-50 steel showed higher fatigue lifetimes with increased compressive surface stress. These are the first data which have shown the beneficial effect of residual stress in RCF testing and which indicate that SiC can be used as a bearing material.

Monolithic liquid phase sintered SiC rods (or monolithic SiC-TiC composite rods) have low fatigue lifetimes due to rapid wear with typical fatigue spalling caused by inherent porosity ($\approx 1\%$). CVD SiC is fine-grained and relatively dense compared to the monolithic SiC. CVD SiC has the advantage that the decreased porosity increases fatigue lifetimes but the disadvantage that the fine-grained microstructure is more brittle. The CVD SiC/SiC rods failed after excessive "wear" due to brittle fracture of the CVD SiC. Increasing the compressive stress for the same CVD SiC, as was the case for the CVD SiC/SiC-30 vol. % TiC rods, eliminated this failure mode. Nine of the 16 rods tested showed no failure and minimal wear after 100 hours of testing. Two of the rods failed due to ball spalling, which also happens with Si_3N_4 . The other five tests were terminated due to spalls which initiated at SiC growth nodules. It is believed that these growth nodules can be eliminated by controlling the CVD process and hence the resulting microstructure. Several vendors who have experience in depositing CVD SiC have indicated that it is possible to minimize the formation of the nodules. A fluidized bed coating technique using CVD SiC on an inexpensive substrate should be investigated to see if the economics are attractive. Further information on this is discussed below.

Slip casting and cosintering was used on three different systems: 1) SiC-15 vol. % TiC/SiC-30 vol. % TiC, 2) $\text{Si}_3\text{N}_4/\text{Si}_3\text{N}_4$ -15 vol. % TiN, and 3) $\text{Si}_3\text{N}_4/\text{Si}_3\text{N}_4$ -20 vol. % TiN. RCF testing showed that the layered ceramics have only marginally better performance as compared to the monolithic ceramics. Fractography indicated that structural defects (i.e., pores and agglomerates) are spall initiation sites in these materials. Improved processing steadily increased the fatigue lifetimes in these materials. RCF testing on the third set of materials (i.e., $\text{Si}_3\text{N}_4/\text{Si}_3\text{N}_4$ -20 vol. % TiN) with improved density ($>99.5\%$ of theoretical) showed no evidence of fatigue spalls.

Cosintering can be used to make materials with high residual compression in the outer layers, but HIPing is still required to eliminate processing flaws, resulting in no economical advantage in using the layered composites. CVD SiC, on the other hand, has not only demonstrated increased RCF lifetimes and may be economically attractive, but also

is a better approach for making uniform layers on balls than a dip-coating cosintering approach.

The objectives of demonstrating increased RCF lifetimes and decreased wear rates have been met during this two year program. The third objective of demonstrating increased reliability should be a natural consequence of iterative testing and it is believed that this can be demonstrated by limiting nodule formation during CVD coating.

The possibility of CVD SiC coated ball bearings using an inexpensive substrate appears to be feasible. It is believed that if the modulus of a carbon/graphite material could be increased to ≈ 200 GPa by mixing in fine SiC to increase the modulus and controlling the thermal expansion with TiC additions, a C-SiC composite could be made in furnaces presently used to form graphite without substantially increasing the cost. Discussions with industry suggest that it should be possible to test this experimentally. If successful, near net shaped balls could be made spherical before inserting them into a fluidized bed CVD reactor. General Atomic has been contacted to assess the cost of fluidized bed CVD coating. Heart valves are commercially coated in a fluidized bed by suspending the valves in a bed of small balls. It is estimated that $\approx 4,000$ 4 mm balls can be coated simultaneously at a cost of \$0.50/ball (using a 25 cm diameter reactor with a 200 cm^3 working volume). This cost could be reduced by a factor of four if a reactor twice the diameter were used. These numbers are only estimates, but it appears that CVD SiC could substantially reduce the cost of ceramic bearings if an inexpensive substrate can be coated. Since graphite is already used in the semiconductor industry and can be coated well with CVD SiC if the thermal expansion mismatch is minimized, it would appear that C-SiC may be a suitable inexpensive substrate when produced in large quantities.

While the SiC/C-SiC balls would be lighter than Si_3N_4 , the only advantage currently of interest is cost. Lower cost is possible due to: a) low cost raw materials and large scale manufacturing typical of the graphite industry, b) elimination of the HIPing step, and c) the ease with which CVD SiC can be finished. There are many unknowns at the present time and further development is necessary before a serious cost assessment can be made. In order to commercialize this technology the following steps should be taken:

- 1) Demonstrate with RCF rod testing that CVD SiC/SiC-TiC rods can be made to last 100 hours (20 out of 20 tests). This would involve coating monolithic SiC and SiC-TiC rods of controlled thermal expansion (i.e., SiC, SiC-10 vol. % TiC, SiC-20 vol. % TiC, SiC-30 vol. % TiC and SiC-40 vol. % TiC) simultaneously.

- 2) Demonstrate that CVD SiC/SiC-TiC balls can be coated in a fluidized bed and compare the ease of finishing these balls with Si_3N_4 balls finished using the same

procedures and equipment. This would tell whether cost estimates for CVD coating are realistic and would show whether there is any cost saving in finishing operations.

3) Demonstrate that C-SiC can be fabricated economically by industry and that the thermal expansion can be controlled. Coat these rods and conduct RCF testing as discussed in step 1 above.

4) Demonstrate that CVD SiC/C-SiC balls can be coated and survive 100 hours at 5.5 GPa in RCF testing.

5) Promote the commercialization of this product by making any patent protection received readily available to companies willing to commercialize the technology.

In summary, compressive residual stresses have been shown to unequivocally increase rolling contact fatigue lifetimes in CVD SiC. It is believed that this is due to increased apparent toughness eliminating spalling. CVD SiC with high compressive stress shows minimal wear. High compressive surface stress (≈ 680 MPa) limits surface pullout. Further development is needed in order to show the feasibility of a low-cost substrate which may make CVD SiC a more economical ceramic rolling element material than Si_3N_4 . While lower cost is the driving force for pursuing further development efforts, other attractive features of these materials would be lower specific gravity and higher resistance to chemical attack. The use of thermal expansion mismatch for introducing high compressive stresses in ceramics improves the performance during rolling contact fatigue and warrants further development.

2. INTRODUCTION

Performance and reliability of many military and industrial systems can be improved significantly by using all-ceramic or hybrid ceramic bearings. Military systems that can benefit from ceramic bearings include inertial guidance instruments, precision sensor gimbals, turbine engine exhaust nozzle actuators, submarine pumps, etc. In the civilian sector, hybrid ceramic bearings have been found to improve system performance in the machine tool industry (extended life spindles, high-speed head options, ultra high speed machining centers and high-speed grinding spindles), chemical processing industry (industrial blower), vacuum pumps, vapor deposition and molecular beam epitaxy equipment, and hot valve and kiln bearings[5]. Ceramics offer such advantages in these bearing applications as high speed and acceleration capability due to reduced centrifugal ball loads of the light weight ceramic materials, reduced wear and extended rolling-contact fatigue life due to the higher hardness and lower coefficient of friction, corrosion resistance and high-temperature capability[5].

A crystallized glass-ceramic, a hot-pressed alumina, and a hot-pressed silicon carbide were investigated for bearing applications in the early 1960s[6-8]. Results of these early tests showed that failure of ceramics was essentially similar to that in bearing steels, i.e. it originated at subsurface flaws, typically pores, located at about the depth of the maximum shear stress. Subsurface cracks developed from these flaws, extended nearly parallel to the surface and eventually formed a spall. None of the ceramic materials tested, however, showed improved fatigue life. The life of the ceramic bearings was less than 10 percent of that of typical rolling-element bearing steels under the same conditions of stress.

The focus of efforts to develop ceramic bearings shifted to silicon nitride in the early 1970s[9-14]. The initial results were, however, mixed. Results of Scott et al.[10,11] and Parker and Zaretsky[12] did not show improved bearing life for silicon nitride. Baumgartner[13,14] demonstrated that 10 % fatigue life of bearing elements made from a hot-pressed grade of silicon nitride was eight times the life of AISI M-50 steel in rolling contact fatigue tests. Material deficiencies in the form of inhomogeneities, such as pores and inclusions, and different surface finishes were probably responsible for the variable results in these early investigations. Optimization of sintering additives, processing, and surface finishing techniques have advanced rapidly in the last decade to a degree that silicon nitride is now considered a viable ceramic bearing material[3,15,16]. A variety of bearing tests with hybrid bearing systems has shown that hot-pressed silicon nitride bearing elements can improve fatigue life by one to two orders of magnitude over equivalent all-steel bearings[16-18]. More recently, strict specifications for bearing-grade

silicon nitride powder and additives[19], use of hot-isostatic pressing as the preferred route for processing[20,21] and application of nondestructive inspection techniques[22] have all contributed to increased reliability and performance of silicon nitride bearings[23].

Despite the advances made in the development of silicon nitride bearings, their use in military applications has been limited. Two major barriers to greater use of ceramic bearings have been their high cost and inadequate reliability[24]. Continued improvements in materials and processing technology and use of reliable, non-destructive inspection (NDI) methods at different stages of manufacturing will no doubt further improve performance and reliability of ceramic bearings. An alternate approach that has potential to significantly enhance bearing element performance and reliability is through introduction of compressive residual stress in the bearing surface. Compressive residual stresses in the contact surface of ball-bearing race grooves have been found to increase the rolling-element fatigue life of steels[25,26]. Ball bearing lives were increased by a factor of two when metallurgically induced compressive residual stress was present in the inner rings[25]. There has not been a similar attempt to take advantage of compressive residual stress in ceramic bearings. Potential for such an approach to improve ceramic bearing life was noted by Baumgartner[14].

Virkar[27] patented a simple technique for introducing compressive residual stresses in ceramics using transformation-induced stresses. Ceramtec, Inc. and the University of Utah used this generic technology to fabricate layered ceramic composites either by powder pressing or slip casting. The compositions of the layers are selected in such a way that outer layers are placed in residual compression either by selective phase transformation of a constituent in the outer layer or by thermal expansion mismatch with the interior layer. Three-layered sandwich composites consisting of alumina and unstabilized zirconia in the outer layers and alumina and fully-stabilized zirconia in the inner layer were fabricated with residual compression in excess of 600 MPa[28-32]. These layered composites have been shown to exhibit high strengths ($\sigma_f = 1274$ MPa in slip-cast composites), high reliability (Weibull modulus, $m = 19$) and excellent damage resistance as evidenced by high strengths in indented specimens ($\sigma_f = 800$ MPa strength at 1000 N Vickers indentation load[31]). A significant fraction of the compressive stress is retained at high temperatures[32].

This report discusses an experimental study funded by the Advanced Research Projects Agency (ARPA) aimed at demonstrating the benefits of surface residual compression in ceramic bearing elements in terms of increased rolling contact fatigue life, decreased wear, and increased reliability (i.e., less scatter in fatigue life). The research focused on the silicon-based ceramic composite systems with either Si_3N_4 or SiC as the

bearing surface. Thermal expansion mismatch between layers yielded surface compression in the range of 100 to 700 MPa. The proposed research was a joint effort between Ceramatec Inc. with Dr. Raymond Cutler as the principal investigator on a prime contract and Prof. Dinesh K. Shetty as the principal investigator on the University of Utah subcontract. Ceramatec led the effort in fabricating layered ceramic composites and bearing elements. Research at University of Utah was directed at characterizing the surface compression and damage resistance of the layered composites. Layered and monolithic bearing rods were also tested at the University of Utah in rolling contact fatigue to assess the effect of surface compression on fatigue life, scatter in fatigue life, and rolling contact wear.

2.1 Research Objectives

The proposed research had two objectives: (1) fabricate layered $\text{Si}_3\text{N}_4/\text{SiC}$ composites in planar and cylindrical geometries using different approaches, and (2) demonstrate the benefits of residual compression in the contact surface in terms of high damage resistance (i.e. high strength of indented bars) and improved rolling contact fatigue life, decreased wear, and enhanced reliability in life relative to the monolithic bearings.

2.2 Technical Background

Strength and Damage Resistance of Layered Ceramic Composites:

As noted above, Ceramatec Inc. and the University of Utah have developed the technology for fabricating layered composites in plate and cylinder geometries with outer layers consisting of alumina and unstabilized zirconia and inner layers made of alumina with stabilized zirconia. On fabrication by either die-pressing or slip-casting and sintering and cool down, the zirconia in the outer layers undergoes transformation from tetragonal to monoclinic polymorph with an accompanying increase in volume. This volume increase is partially constrained by the inner layer resulting in high compression in the thin outer layers and balancing low tension in the thick inner layer[28,29]. Measurements by a strain-gage technique[1] indicate that residual compression of 600 MPa can be developed by this approach[32,33]. Figure 1 shows linearized Weibull plots of fracture stresses of monolithic outer, monolithic inner and three-layer composite ceramics fabricated by dry pressing as well as slip casting. It is noted that the three-layer composites exhibit both increased strengths as well as increased Weibull moduli relative to the monolithic ceramics. Improvements in uniformity of the thicknesses of the layers by slip casting have resulted in composites exhibiting strengths in excess of 1 GPa[32].

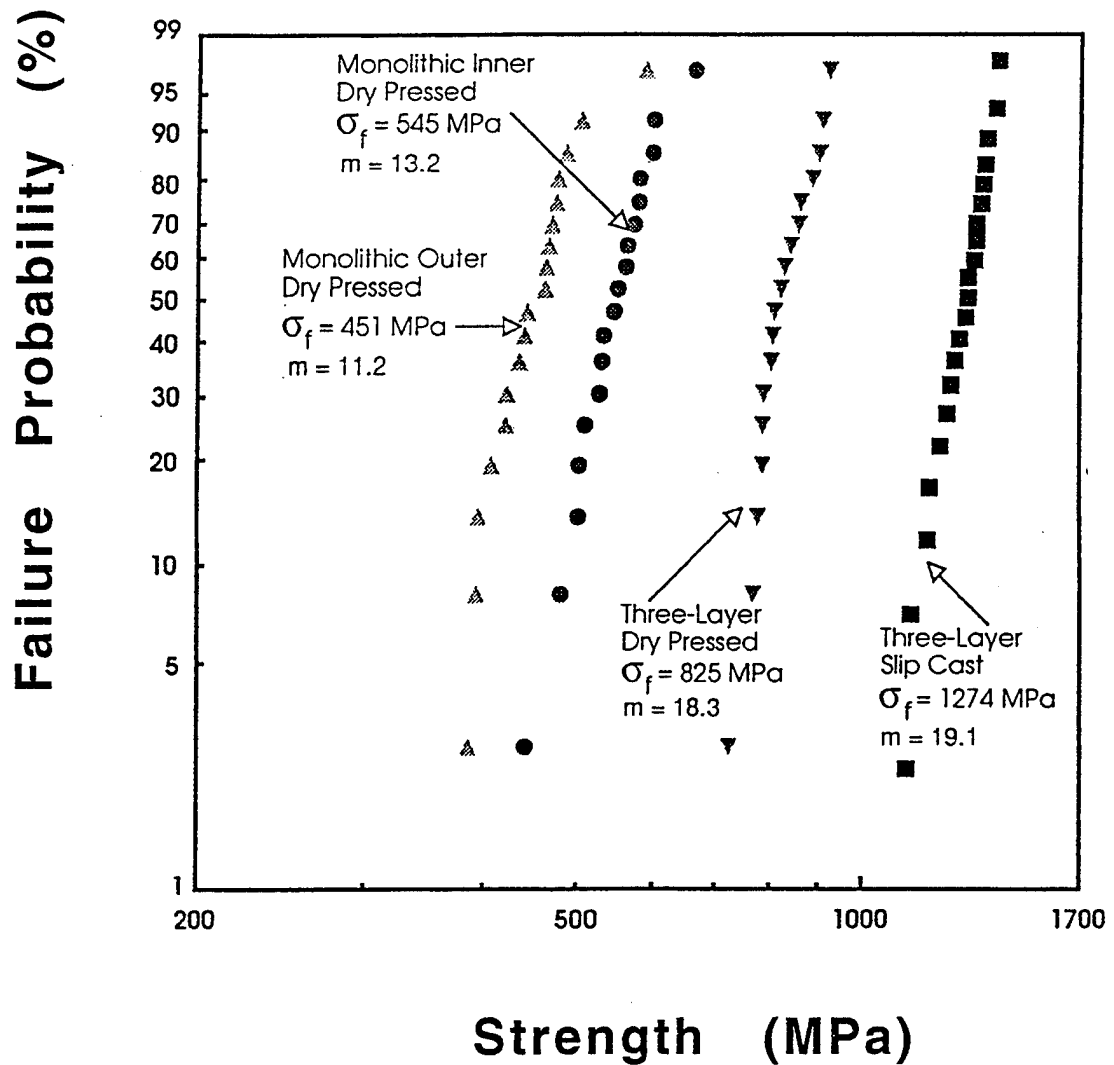


Figure 1. Linearized Weibull plots of fracture stresses (four-point bend strength) of monolithic and three-layer zirconia-toughened alumina composites.

The increased Weibull modulus of the three-layer composites is due to the presence of the residual compression. This can be easily demonstrated by superposition of the stresses. First, it is assumed that the difference between the mean fracture stresses of the dry-pressed monolithic outer material and the dry-pressed three-layer composite (i.e., $825 - 451 = 374$ MPa) is the compressive stress in the outer layers. If this stress is now added to each fracture stress of the monolithic outer material, the resulting strength distribution corresponds to a Weibull modulus of 17.6, in close agreement with the measured Weibull modulus of 18.3. This exercise demonstrates that deliberate introduction of residual

compression on the surface of structural ceramics can be a viable approach to increase both the Weibull modulus (i.e., reliability) and the strength.

It is well known that in brittle materials, however, it is not the strength of the as-fabricated material that is significant, since contact damage in service can severely degrade the strength via flaw generation. A more meaningful assessment of a brittle material's applicability in contact loading conditions, such as in bearing elements, should be based on its damage resistance, i.e., ability to sustain strength following contact damage. A remarkable feature of the layered composites is their excellent damage resistance[31]. This is demonstrated in Figures 2 and 3 for three-layer composites made of zirconia-toughened alumina (ZTA). Figure 2 compares the decrease in four-point bend strength of the three-layer composites of ZTA with increasing load used in indentation with a Vickers diamond pyramid indenter with the corresponding decreases in strength of the monolithic ceramics of the inner and the outer layers. At the maximum indentation load of 1000 N the strengths of the monolithic ceramics decreased from an initial strength of 900 MPa to less than 150 MPa, while the three-layer composite sustained a strength of nearly 800 MPa.

Indentation with the Vickers diamond pyramid produces two orthogonal half-penny shaped cracks. The fracture response of these cracks has been modelled by Hansen et al.[31] using indentation fracture mechanics theory. The strength of a three-layer composite ceramic in which the outer layer thickness is much greater than the depth of the half-penny crack is given by the following equation :

$$\sigma_f = \frac{C K_{IC}^{\frac{4}{3}}}{\left[\frac{E}{H} \right]^{\frac{1}{6}} P^{\frac{1}{3}}} - \sigma_r \quad (1)$$

where

- σ_f = fracture strength of the indented ceramic,
- C = a nondimensional constant dependent on the indenter geometry, ~ 2.02 ,
- K_{IC} = fracture toughness of the ceramic,
- E = elastic modulus of the ceramic,
- H = hardness of the ceramic,
- P = indentation load,
- σ_r = residual stress in the outer layer of the three-layer composite.

The linear relation between strength and $P^{-1/3}$ noted in Figure 3 is consistent with Equation (1). The parallel shift of the strength plot toward higher strengths for the three-layer composites relative to the monoliths reflects a high compressive stress (σ_r is negative) in the outer layers. The intercept on the strength axis obtained by extrapolating the straight

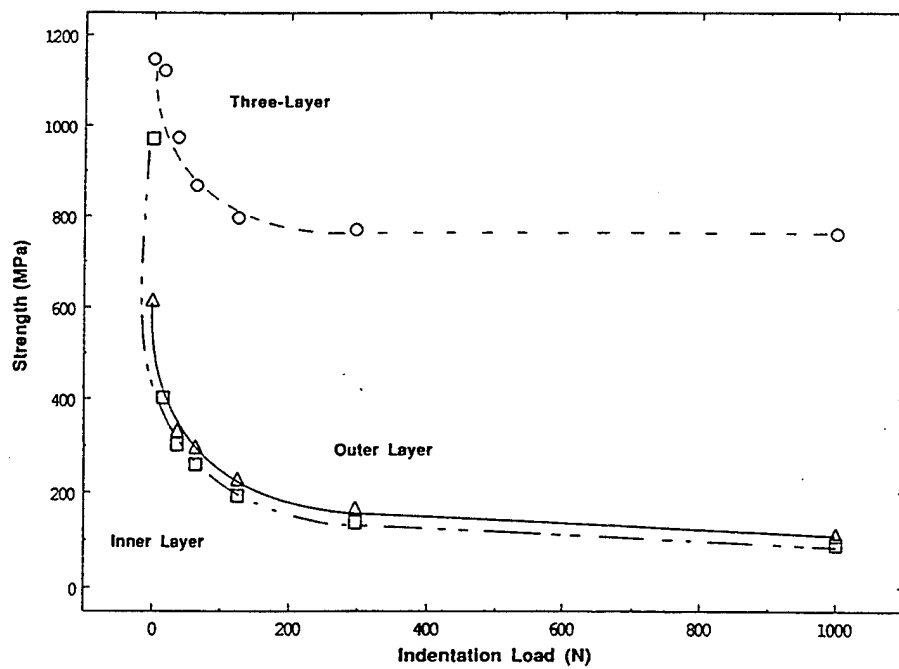


Figure 2. Decrease in fracture strengths of slip cast three-layer and monolithic zirconia-toughened alumina ceramics with increasing indentation loads.

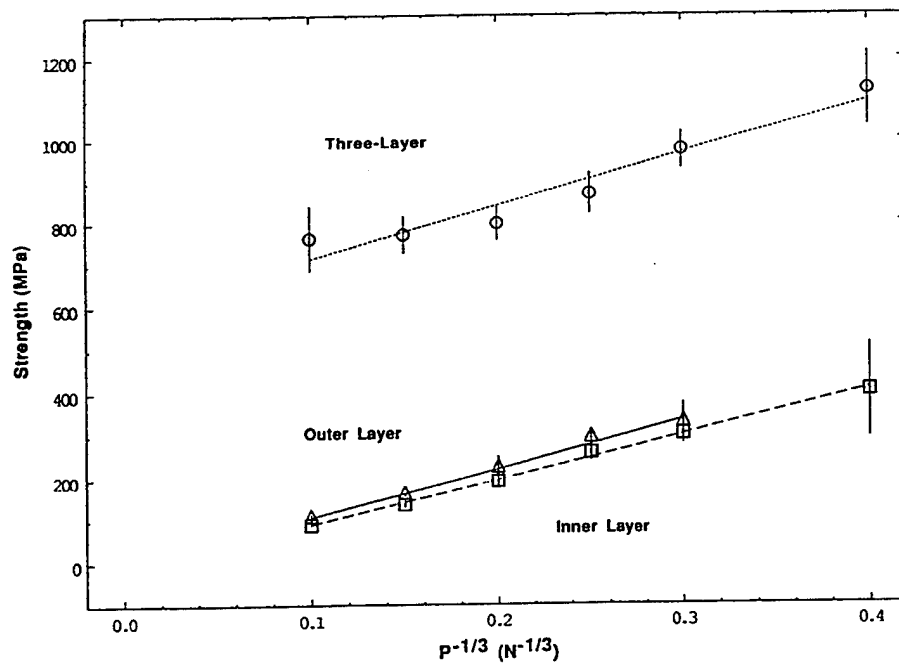


Figure 3. Fracture strengths (σ_f) versus inverse cube root of indentation load ($P^{-1/3}$) plots for slip cast three-layer and monolithic ZTA ceramics.

line fit gives a measure of the residual stress, σ_r . It is noted in Figure 3 that the three-layer composites of ZTA exhibit a residual compression of nearly 650 MPa.

Compressive Residual Stress in a Two-Layer Ceramic Bearing:

Residual stresses can also be generated in ceramics via controlled thermal expansion mismatch. Figure 4 shows a scheme for introducing residual compression in the outer layer of a two-layer ceramic roller bearing 9.525 mm (3/8 inch) in diameter and 76.2 mm (3 inch) long. The outer layer is assumed to be 250 μm in thickness and made of Si_3N_4 with the following properties : $E_1 = 320 \text{ GPa}$, $\nu_1 = 0.2$, $\alpha_1 = 3.4 \times 10^{-6}/^\circ\text{C}$. The inner core will be designed to be made of SiC with the following properties : $E_2 = 420 \text{ GPa}$, $\nu_2 = 0.2$, $\alpha_2 = 4.5 \times 10^{-6}/^\circ\text{C}$. If the interface between the layers is strongly bonded, the residual stresses in the two-layer cylinder are given by the 'bead-seal' solutions[34]. Figure 5 shows the expected variation of residual stresses along a radius in the outer layer and part of the inner layer on cooling a composite cylinder from a fabrication temperature of 1000°C . The residual stresses are axisymmetric and independent of angular position. It is noted that the outer layer is placed in a state of nearly equibiaxial compression with the axial and tangential stresses of about 400 MPa. A residual tensile stress does arise in the radial direction, but its maximum value is only about 23 MPa and it occurs at the interface.

The temperature range of cooling, i.e., $\Delta T = 1000^\circ\text{C}$, used in the above calculations was based on an anticipated chemical vapor deposition temperature for depositing Si_3N_4 on a SiC substrate. If the two-layer roller bearing is fabricated via slip casting and sintering route, the applicable temperature range for residual stress build-up would be much higher and, accordingly, much higher residual stresses can be expected.

Effect of Compressive Residual Stress on Rolling Contact Fatigue Life of Ceramic Bearings :

Fatigue life of a rolling element is defined as the total number of contact stress cycles sustained before failure, i.e., the element shows evidence of surface damage in the form of a spall or a crack. A large body of test data on both bearing steels and ceramics indicates that fatigue life of bearing elements is inversely proportional to the maximum contact stress, p_{max} , to a power n [24] :

$$\bar{L} = \frac{A}{p_{\text{max}}^n} \quad (2)$$

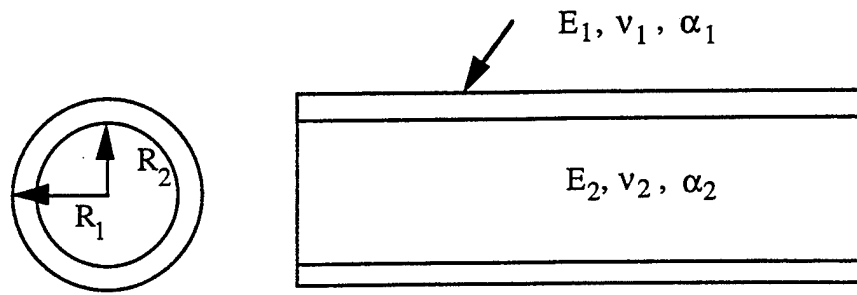


Figure 4. Schematic of a two-layer roller bearing consisting of Si_3N_4 outer layer and SiC inner layer.

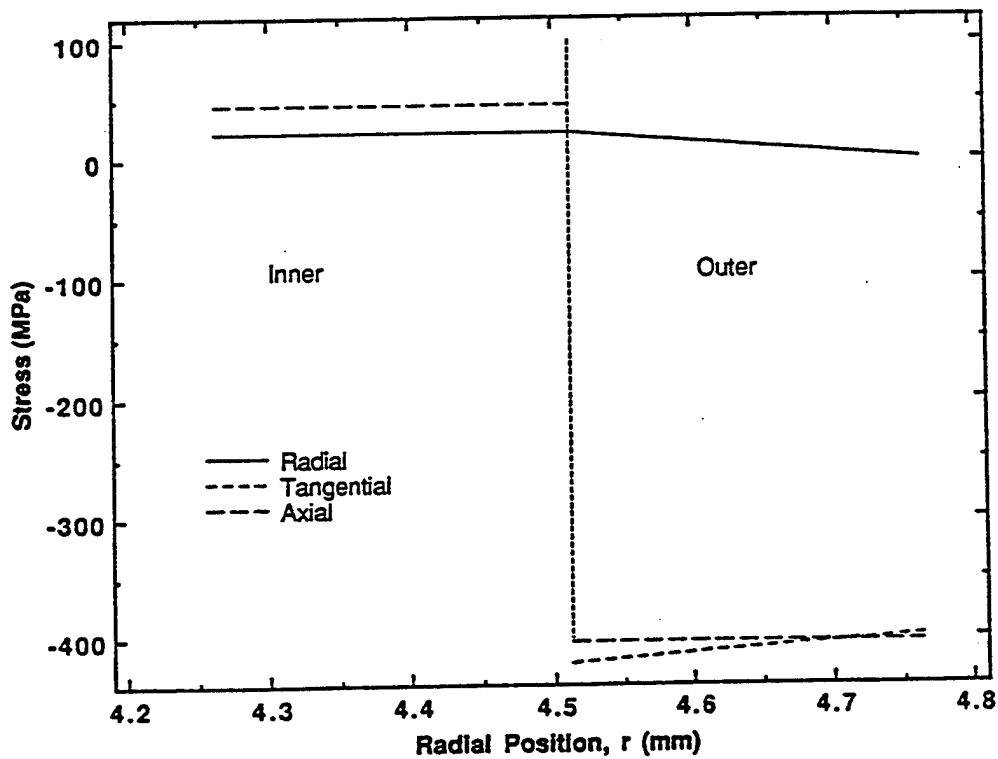


Figure 5. Variation of radial, tangential and axial stresses along a radius in the outer layer and part of the inner layer of a two-layer $\text{Si}_3\text{N}_4/\text{SiC}$ roller bearing.

In Equation (2), L is the fatigue life in stress cycles for failure of a selected fraction of bearing elements (typically 10 %) and A and n are empirical constants established from the test data. For bearing steels, the stress exponent n is typically 9 to 10. Ceramics exhibit a range of n values from 7 for sintered alumina to 16 for silicon nitride[24]. A glass-ceramic, SiC and nickel-bonded TiC have shown intermediate values.

In bearing steels, it is believed that the maximum shear stress is the most significant stress in initiating the fatigue cracks. This is supported by the fact that subsurface cracks which finally lead to spalling are typically located at a depth roughly corresponding to the location of the maximum shear stress. Accordingly, the effect of a residual stress on fatigue life has been rationalized in terms of a modified maximum shear stress[35] :

$$\bar{L} \propto \left[\frac{1}{(\tau_{\max})_r} \right]^n \quad (3)$$

where $(\tau_{\max})_r$ is the maximum shear stress modified by the residual stress according to the equation[35] :

$$(\tau_{\max})_r = \tau_{\max} + \frac{1}{2} (\pm \sigma_r) \quad (4)$$

In Equation (4), τ_{\max} is the maximum shear stress in the absence of a residual stress and σ_r is the residual stress. The positive and negative signs indicate a tensile and a compressive residual stress, respectively.

The mechanism(s) of fatigue crack nucleation and growth have not been established as yet for ceramic bearing elements. The appearance of fatigue damage in the form of spalls in ceramic bearings has been claimed to be similar to those observed in bearing steels[24]. If ceramic bearing surfaces with compressive residual stresses respond in the same manner as do bearing steels, then Equations (3) and (4) predict significant improvement in bearing life. For example, for the two-layer ceramic bearing discussed in the previous section, a compressive residual stress of 400 MPa would increase fatigue life by a factor of 5.5 for a stress exponent of 16 for Si₃N₄ at the Hertz contact stress of 5.93 GPa. The contact stresses used in rolling contact fatigue testing are typically much higher than actual stresses in bearings in order to accelerate failure and, therefore, the projected life improvements for bearings are higher. These projections of life improvements should be taken only as rough estimates since both the mechanism(s) that control fatigue lives and the significant stress that influences fatigue life are not well established for ceramics.

2.3 Proposed Research

The two tasks shown below were proposed to and funded by ARPA. They are included below for those interested in comparing the proposed research with that which was actually performed.

TASK 1 : *Approaches for Introducing Compressive Residual Stresses and Rationale for Selecting Ceramic Compositions for Layered Composites.*

There are two basic approaches that can be used to generate residual compression in the outer layers of layered ceramic composites. The first approach makes use of transformation of a dispersed phase in the outer layers on cooling from the fabrication temperature. The selected phase transformation involves a volume expansion which is partially constrained by the inner layer, thus placing the outer layer in compression. The magnitude of the compression is dependent on the volume expansion of the transforming phase, its volume fraction, elastic properties of the ceramic layers, the geometry of the layered composite and temperature[28,29]. Ceramtec, Inc. has extensive experience in using this approach to fabricate strong (strengths exceeding 1 GPa) and damage-resistant layered composites consisting of alumina with unstabilized zirconia phase in the outer layers and alumina and stabilized zirconia in the inner layer. The unstabilized zirconia in the outer layer undergoes a tetragonal to monoclinic phase transformation with an accompanying volume expansion of about 4% typically over a temperature range of 650 to 750 C.

The second approach for introducing compressive residual stress makes use of thermal expansion mismatch between the outer and the inner layers. The compositions are selected to obtain a lower coefficient of thermal expansion for the outer layers and a higher coefficient of thermal expansion for the inner layer. Following fabrication and consolidation at a high temperature and cooling to room temperature the outer layers are placed in compression. The magnitude of the compression is dependent on the thermal expansion mismatch in addition to such factors as elastic properties, geometry and temperature range of cooling from the fabrication temperature.

The latter approach is attractive for designing layered composites of covalently-bonded ceramics such as Si_3N_4 . Si_3N_4 is a good choice for the outer bearing layer because of its proven performance as a rolling contact bearing material and its low thermal expansion ($\alpha = 3.2 \times 10^{-6}/^\circ\text{C}$). The inner layer can be made from SiC which has a higher thermal expansion ($\alpha = 4.5 \times 10^{-6}/^\circ\text{C}$) as compared to Si_3N_4 . Ceramtec has developed a liquid-phase sintered SiC[4,36,37]. The advantage of the liquid-phase sintered SiC is its ease of sintering. SiC with greater than 98% theoretical density can be produced by sintering for 5 minutes at 2000°C. Although this SiC has excellent erosion resistance[38] it

is much lower in toughness than Si_3N_4 . The two-layer approach is an excellent concept for improving the apparent toughness of SiC. The thermal expansion of the inner layer of two-layer composites can be increased further, if necessary, by adding Al_2O_3 . Recent data[39] suggest that the same SiC- Y_2O_3 - Al_2O_3 system can be used to make higher toughness ($K_{\text{IC}} \sim 6 \text{ MPa}\cdot\sqrt{\text{m}}$) SiC. A potential advantage of making layered bearings is that materials other than silicon nitride can be used and still achieve significant bearing life due to surface compression. Current methods of fabricating silicon nitride bearings are expensive because of the encapsulated HIPing that is required. Potential substitution with SiC is also attractive from a hardness point of view because life of Si_3N_4 bearings is increasingly limited by wear.

Task 1 will consist of making monolithic and three-layer strength bars of candidate materials. The objective of this task will be to determine effective methods for introducing compressive stress on the order of 400 MPa in the outer layers of three-layer composites. Si_3N_4 will be used as the outer-layer material. It can be either applied to dense substrates by chemical vapor deposition (CVD) or co-sintered with the inner-layer material.

The work of Torti and Richerson[40] demonstrated that substantial compressive stresses can be introduced in hot-pressed, three-layer Si_3N_4 -SiC- Si_3N_4 composites. However, expensive processing techniques, such as glass-encapsulated HIPing or hot pressing, are not very desirable from a cost point of view. Monolithic inner-layer materials will be fabricated using the liquid-phase sintering process developed at Ceramtec[4, 36, 37]. The liquid-phase sintering process involves the addition of oxides, i.e., Al_2O_3 and Y_2O_3 , to either α -SiC or β -SiC powders. Conventional forming techniques are followed by heating above the eutectic temperature of the oxide-based liquid. The bars will then be ground and polished to a 1 μm finish to simulate the finish on roller bearing elements. A 250-300 μm thick outer Si_3N_4 layer will then be applied using CVD at rates of 25 $\mu\text{m}/\text{hour}$ for amorphous Si_3N_4 or 50 $\mu\text{m}/\text{hour}$ for crystalline Si_3N_4 at Midland Materials Research, Inc. CVD layers will initially be applied at 1050-1100 C.

Dense CVD Si_3N_4 coatings have been applied on reaction-bonded silicon nitride and graphite resulting in highly wear-resistant surfaces[41]. The adherence of the CVD Si_3N_4 to a polished surface should be excellent. This will be confirmed by an examination in the scanning electron microscope(SEM). Amorphous films have excellent surface finish and it may not be necessary to repeat final polishing after the CVD step. It is anticipated that lapping/polishing will be performed by R & D Engineering at Orem, Utah, using state-of-the-art lapping procedures. If their surface finish is unacceptable, ceramic bearing companies experienced in surface finishing, for example, CERBEC (Ceramic Bearing

Company), will be contacted to produce the required surface finish for the rolling contact fatigue test rods.

The residual stress in the outer layers of a planar three-layer composite is given by the following equation[28] :

$$\sigma_1 = \frac{E_1 (\alpha_1 - \alpha_2) \Delta T}{\left[\frac{2 E_1 d_1 (1 - \nu_2)}{E_2 d_2} + (1 - \nu_1) \right]} \quad (5)$$

where E , ν and α are, as before, Young's modulus, Poisson's ratio and coefficient of thermal expansion, respectively, d is the individual layer thickness and the subscripts 1 and 2 refer to the outer and the inner layer, respectively. Note that for $\alpha_1 < \alpha_2$, σ_1 is negative, i.e. a residual compression develops in the outer layers. Taking the appropriate values for E , ν and α for Si_3N_4 (outer layer) and SiC (inner layer) as before (see page 7), a 250 μm thick Si_3N_4 outer layer on a 4 mm thick bar results in a residual compression of 397 MPa in the outer layers. The balancing tensile stress in the inner layer is 57 MPa. The magnitude of the residual stress in the outer layer will be varied by controlling the outer-layer thickness via the CVD coating time.

Si_3N_4 - SiC - Si_3N_4 composites will also be prepared by making three-layer bars in the green state using Si_3N_4 - Y_2O_3 - Al_2O_3 powder for the outer layers and SiC - Y_2O_3 - Al_2O_3 for the inner layer. The strength bars will be pressureless sintered to closed porosity using the sintering conditions developed for SiC and they will then be cladless HIPed in argon at 1800 C for 10 minutes. If this approach does not work for making dense Si_3N_4 , glass encapsulation will be used to densify the bars.

Alternate inner-layer materials (Si_3N_4 - TiN - Y_2O_3 - Al_2O_3 , SiAlON - TiN - Y_2O_3 , Si_3N_4 - SiC - YAG , etc.) will be evaluated, as necessary, if the liquid-phase silicon carbide system does not yield the desired compressive stress. The composition of the inner layer will be tailored to get a thermal expansion of $4.5 \times 10^{-6}/\text{C}$ with the objective to create a material which is compatible with the CVD Si_3N_4 coating or one which can be co-sintered (or co-HIPed) with Si_3N_4 .

Task 1 will consist of making monolithic and three-layer strength bars of candidate materials and characterizing these materials. The thermal expansion of dense monolithic bars will be determined using dilatometry in the temperature range from room temperature to 1200 C. Several candidate materials will be coated with CVD Si_3N_4 simultaneously. Groups of bars will be removed from the CVD chamber at various times to obtain bars with outer Si_3N_4 layers of ~100, ~200 and ~300 μm thickness. It is anticipated that several CVD cycles will be made in order to optimize the coating process. Residual stresses in the

three-layer composites will be characterized using strength, indentation, strength/indentation, and strain gage techniques, as have been performed previously for Al_2O_3 -15 vol. % ZrO_2 composites[28-33]. The measured stresses will be compared with calculated stresses. Fractography will be used to identify fracture origins and failure modes.

An iterative approach will be used to optimize the monolithic and layered composites. Task 1 will identify material systems which give enhanced strength, greater reliability and higher apparent toughness by placing the outer Si_3N_4 layer in compression.

TASK 2 : *Development of Approaches for Fabricating Layered Composites in Planar and Cylindrical Geometries.*

The objective of Task 2 is to make layered cylindrical rods (and, if required, three-layer plates) for rolling contact fatigue and wear tests to be conducted at a place to be designated by Wright Patterson Air Force Base. Two approaches will be investigated for making layered composite cylinders : 1) chemical vapor deposition (CVD) of outer layers on sintered and surface-finished monolithic inner material, and 2) fabrication of both the inner and the outer layers in the green state by slip casting and cosintering. Task 1 will identify the materials used in Task 2. Until further direction is obtained from Task 1, efforts in Task 2 will be devoted to developing the correct rheology for slip casting Ceramtec's liquid-phase sintered SiC , since slip casting will be the primary method for fabricating cylindrical geometries. Ceramtec has extensive experience in slip casting monolithic and layered plates, tubes, and solid cylinders of Al_2O_3 , ZrO_2 and Al_2O_3 - ZrO_2 composites. Slip casting of layered composites has been accomplished by preparing slips of the outer and the inner materials. The outer layer slip is poured into the mold first and allowed to form a layer of a given thickness, which is controlled by the rheology of the slip and the casting time. The remaining slip is then poured from the mold and the inner layer slip is quickly poured into the mold. In the case of solid plates and cylinders, the inner layer slip is left long enough so that a solid inner layer is formed. For hollow cylinders, as is the case of cam followers, the slip used to form the inner layer is poured out after a given time, and the outer layer slip is again poured in to form the desired thickness of the outer layer on the inner diameter.

The techniques for slip casting solid plates and cylinders are fully developed and can be applied directly to different materials once the correct rheology of the new slips has been determined. Slip-cast components will be dried and pressureless sintered. Post-sintering HIPing will be either cladless or will use glass encapsulation depending on the

density achieved in sintering. One objective of the proposed work is to develop pressureless-sintered, layered ceramic bearings with surface compression which exceed the performance of the state-of-the-art Si_3N_4 bearings (which are HIPed by glass encapsulation). Pressureless sintering has the potential to lower the manufacturing costs of ceramic bearings.

Two-layer composites as well as monolithic outer and inner layer materials will be fabricated by slip casting. After sintering, grinding and polishing, CVD coatings will be applied to selected inner layer samples to compare the two fabrication approaches.

The magnitude of the residual stresses introduced in the rollers will be determined by strength testing. Indentation/strength testing will be used to determine their damage resistance and screen candidate materials for fatigue testing.

Table 1 shows a time table for completing the tasks of the proposed research over an anticipated performance period of 24 months.

Table 1
Time Table for Proposed Research

<u>Task</u>	Months From Project Start													
	0	2	4	6	8	10	12	14	16	18	20	22	24	
1. Fabrication of SiC Bars	----->													
1. Initial CVD Trials and Characterization			----->											
1. Co-sintering of Si ₃ N ₄ -SiC-Si ₃ N ₄			----->											
1. Iterative Processing and Other Composites As Necessary				----->										
2. Slip Casting of SiC			----->											
2. Fabrication of Rollers and Plates Based on Input from Task 1					----->									
1, 2. Grinding, Lapping and Polishing			----->											
2. SEM Evaluation						----->								

3. EXPERIMENTAL PROCEDURES

Commercially available powders were processed, generally in water, by adding a dispersant and milling for 16-24 hours using either SiC or ZrO₂ media. Viscosity and pH were used to monitor and control the dispersibility of the ceramic suspensions. Solid contents were generally between 30 and 40 vol. %. The milled slurries were passed through a 45 μ m screen and then treated with an ultrasonic probe for 5 minutes while stirring. Casting was performed in plaster molds after deairing the slip. When two-layer rods were cast, the outer-layer slip was poured into the mold for a specified period of time, quickly decanted, and the inner-layer slip was poured into the same mold. The cast parts were air dried and then slowly heated ($\approx 2^\circ\text{C/hr}$) to 110°C in air. The dried parts were loaded into a graphite crucible and heated under an inert environment to the sintering temperature. In the case of Si₃N₄ based materials, BN-Si₃N₄ embedding powder was used to suppress volatilization. Selected samples were cladless HIPed in N₂.

Chemical vapor deposition (CVD) of Si₃N₄ or SiC was performed by three companies: Astro Technologies (Bay City, MI), Ultramet (Pacoima, CA) and Du Pont Lanxide Corporation (Newark, DE). All deposition temperatures were near 1000°C .

Density was measured by water displacement. Plates were sliced and then ground into bars $\approx 3.5 \text{ mm} \times 4.5 \text{ mm} \times 50 \text{ mm}$. The ground bars were chamfered prior to testing in four point bending using a 20 mm loading span and a 40 mm support span at a constant crosshead speed of 0.5 mm/min. on a universal testing machine. A Vickers diamond pyramid indenter with the standard geometry (apex angle of 136°) was used for indenting at a speed of 0.05 mm/min. A drop of dry mineral oil was placed at the site of the indentation before loading to minimize postindentation subcritical crack growth from moisture. Fractography was used to insure that indentation/strength bars failed from the indent. Thermal expansion was assessed in Ar between 20 and 1200°C using a push-rod dilatometer at a heating rate of 2°C/minute .

A technique developed by Virkar [1] was used to measure $\Delta\epsilon_0$, the strain mismatch between the coating and the substrate. The technique is based on measurements of strain, ϵ_M , on one outer surface of a three-layer bar while the outer layer is incrementally removed by grinding. The following equation describes the variation of ϵ_M as a function of δ , the thickness of the outer layer removed by grinding[1] :

$$\epsilon_M(\delta) = \frac{\Delta\epsilon_0 d_2 \delta}{(d - \delta)^2} \frac{(2d + \delta)}{d} \quad (6)$$

In Eq.(6), d is the initial total thickness of the three-layer sandwich plate and d_2 is the inner-layer thickness. The $\Delta\epsilon_0$ values are obtained by fitting Equation (6) to the $\epsilon_M(\delta)$ versus δ data for $\delta < (d-d_2)/2$. Compressive stress was calculated by substituting $\Delta\epsilon_0$ for $\Delta T\Delta\alpha$ in Equation (5) with Young's modulus values either based on literature values or measured experimentally using a strain gage attached to a strength bar and loaded elastically in four-point bending.

Optical and scanning electron microscopy (SEM) was used to assess the thickness of coated samples. SEM was also used to assess wear tracks and to determine fracture initiation sites. A surface profilometer was also used to monitor wear. Electron microprobe was used to look at the chemical variation across interfaces. Selected samples were etched in boiling Murakami's etchant (10 g NaOH and 10 g $K_3Fe(CN)_6$ in 100 ml H_2O) for 30 minutes to delineate grain shape.

The rolling-contact fatigue was measured at the University of Utah using the three-ball-on-rod rolling-contact fatigue test machine described by Glover[2]. The schematic of Figure 6 illustrates the specimen and the three-ball loading arrangement. The 9.5 mm cylindrical test specimen was rotated at 3600 rpm with a direct-drive electric motor mounted in line with the specimen below a table. The specimen was alternately stressed by rolling contact with the three radially-loaded balls. The three balls, separated by a retainer, were radially loaded against the test specimen by two tapered bearing cups thrust-loaded by three compression springs. An accelerometer coupled with a shutdown device monitored the vibration of the cup housings. When a preset vibration level was exceeded, indicating the presence of a surface crack or fatigue spall, the motor automatically stopped. The test duration was measured by an hour meter connected electrically to the motor. Lubrication was applied by a drip feed to the end of the test specimen. The rolling-contact wear on both the balls and the rod was assessed by measuring weight loss.

All the RCF rods were circumferentially ground by a vendor following a specific procedure developed by the manufacturer of the RCF test machine[42]. The grinding involved three stages: rough, intermediate and finish grinding. The rough grinding reduced the diameter in three stages of decreasing feed per pass to 10.033 mm (0.395 in) using a 150-mesh diamond-grit wheel. The intermediate grinding reduced the diameter in three stages of decreasing feed per pass to 9.5504 mm (0.376 in) using 320-mesh diamond-grit wheel. The finish grinding used 500-600 mesh diamond-grit wheel and 2.54 μm per 2 passes to reach the final diameter of 9.525 mm. The specifications for the surface finish were as follows: final diameter = 9.525 mm + 0.000 mm - 0.01 mm, roundness = 0.00127 mm and surface roughness, $RQ = 0.1 \mu m$. Surface profilometry was used to

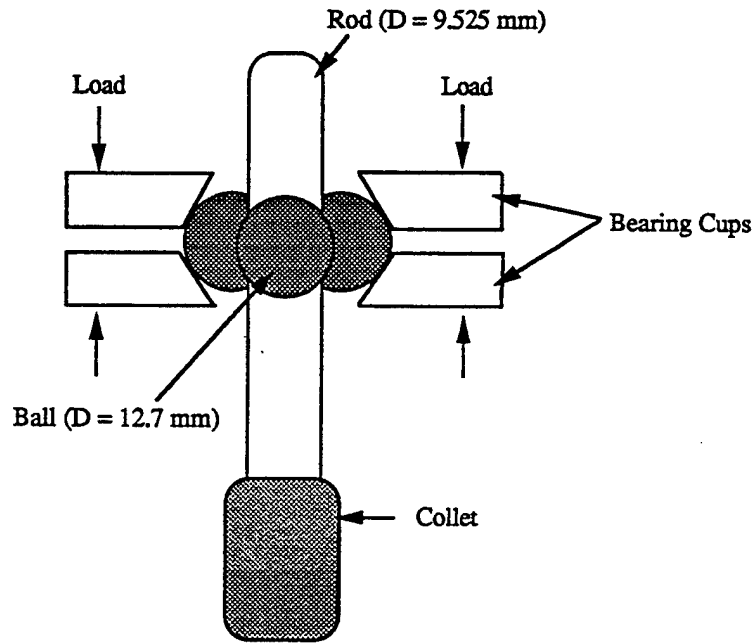


Figure 6. A schematic of the three ball-on-rod rolling contact fatigue test machine.

assess the surface finish of the as-ground rods, as well as tested rods. Weight loss of both balls and rods were used to assess wear.

4. RESULTS AND DISCUSSION

4.1 Materials Selection and Rheology Development

The requirements for successful cosintering are believed to be: 1) ability to control thickness of coating in green state, 2) similar green densities and sintering regimes for outer and inner layer materials, 3) good bonding at interfaces, 4) thermal expansion mismatch ($0.5\text{-}1.0 \times 10^{-6}/^{\circ}\text{C}$) to give compressive stress of 400-800 MPa, 5) moderate to high strength outer layer material and high strength inner material, 6) thickness uniformity, and 7) sharp interface (preferred).

The first requirement is easily accomplished using a slip casting approach. The second requirement, however, is not easily attained due to differences in dispersibility, leading to variable green densities, as well as different sintering regimes. Despite the fact that both SiC and Si₃N₄ can be sintered with liquid phases which are primarily yttrium aluminates or yttrium aluminosilicates, they cannot be sintered in the same temperature range. Si₃N₄ begins sintering at 200-300°C prior to SiC and decomposes in the absence of a nitrogen overpressure. The substitution of AlN for Al₂O₃ in liquid phase sintered SiC[43,44] allows better sintering in N₂, but does not overcome the sintering temperature incompatibility. It was not possible to simply increase the amount of yttrium aluminates in the inner layer since diffusion of liquids is fast and sharp interfaces are not formed as illustrated below by Si₃N₄ compositions with different amounts of sintering additives. Efforts to cosinter SiC and Si₃N₄ were discontinued due to the difficulties associated with this approach.

Table 2 shows the compositions of two slips which were prepared at 70 wt. % solids (40-41 vol. % solids). Viscosities were similar (11-44 mPa·s) for both slips. The

Table 2
Si₃N₄ and Si₃N₄-Y₃Al₅O₁₂ Compositions

Designation	Composition				T.D. ^a (g/cc)
	Si ₃ N ₄ ^b	Al ₂ O ₃ ^c	Y ₂ O ₃ ^d	YAG ^e	
RC2-118B (outer layer)	88.00	3.00	9.00	0.00	3.32
RC2-120A (inner-layer)	76.37	2.60	7.81	13.22	3.44

a. Theoretical density of unsintered body.

b. Kemanord grade H95

c. Reynolds grade HP DBM.

d. Molycorp grade 5600.

e. Prepared by milling Y₂O₃ and Al₂O₃ powders, calcining, and remilling.

Table 3
Characterization of Si₃N₄ and Si₃N₄-Y₃Al₅O₁₂ Compositions

Designation	Code	Shrinkage (%)	Density (g/cc)	Flexural Strength (MPa)
RC2-118B	O	13.4	3.13	734±93 (11)
RC2-120A	I	12.6	3.34	535±115 (6)
Three-layer (≈1/3-1/3-1/3)	O-I-O	13.8	3.23	721±37 (5)
Three-layer (≈1/12-5/6-1/12)	O-I-O	13.8	3.31	705±129 (6)

slip casting time was controlled such that three-layer bars were made with outer layers either 1/3 or 1/12th the total thickness of the bars. Monolithic and three-layer bars were sintered at 1750°C for 3 hours in flowing N₂. The expected thermal expansion mismatch between the outer (Si₃N₄-9 wt. % Y₂O₃-3 wt. % Al₂O₃) and the inner ((Si₃N₄-9 wt. % Y₂O₃-3 wt. % Al₂O₃)-10 vol. % YAG) compositions was ≈5x10⁻⁷/°C. Strength data, listed in Table 3, showed no support for the existence of residual stresses in the layered composites. Despite a distinct color change between the outer and the inner layers, electron microprobe measurements showed that no sharp interface existed (see Figure 7). The lack of a sharp interface is consistent with low melting point eutectics in the SiO₂-Y₂O₃-Al₂O₃ system (see Figure 8) allowing fast diffusion. For this reason, addition of second phases, such as TiN for Si₃N₄, or TiC for SiC, are much better choices than yttrium aluminates (i.e., Y₃Al₅O₁₂, YAlO₃, or Y₄Al₂O₉) for creating high residual stresses in layered composites. The average thermal expansion coefficients, α, over a range of 22-1200°C, of RC2-118B and RC2-120A were identical at 4.2x10⁻⁶/°C. Therefore, even if the diffusion of oxide additives had not taken place, there would not have been any residual stresses in the three-layer composites shown in Table 3.

TiN is often added to Si₃N₄ to make it electrically conducting so that electron discharge machining is possible[46-48]. The purpose of adding TiN to Si₃N₄ in the present work was to increase its thermal expansion coefficient. Assuming a thermal expansion of 3.5x10⁻⁶/°C for Si₃N₄ with Y₂O₃ and Al₂O₃ additions, and 9.0x10⁻⁶/°C for TiN[49], silicon nitride composites with 10, 15, and 20 vol. % titanium nitride, would have thermal expansion coefficients of 4.1x10⁻⁶/°C, 4.3x10⁻⁶/°C, and 4.6x10⁻⁶/°C, respectively, assuming rule-of-mixtures. TiC has been added to SiC to improve mechanical properties[50]. Assuming a thermal expansion of 4.5x10⁻⁶/°C for SiC and 8.5x10⁻⁶/°C for TiC[51], silicon carbide composites with 10, 20, and 30 vol. % TiC would

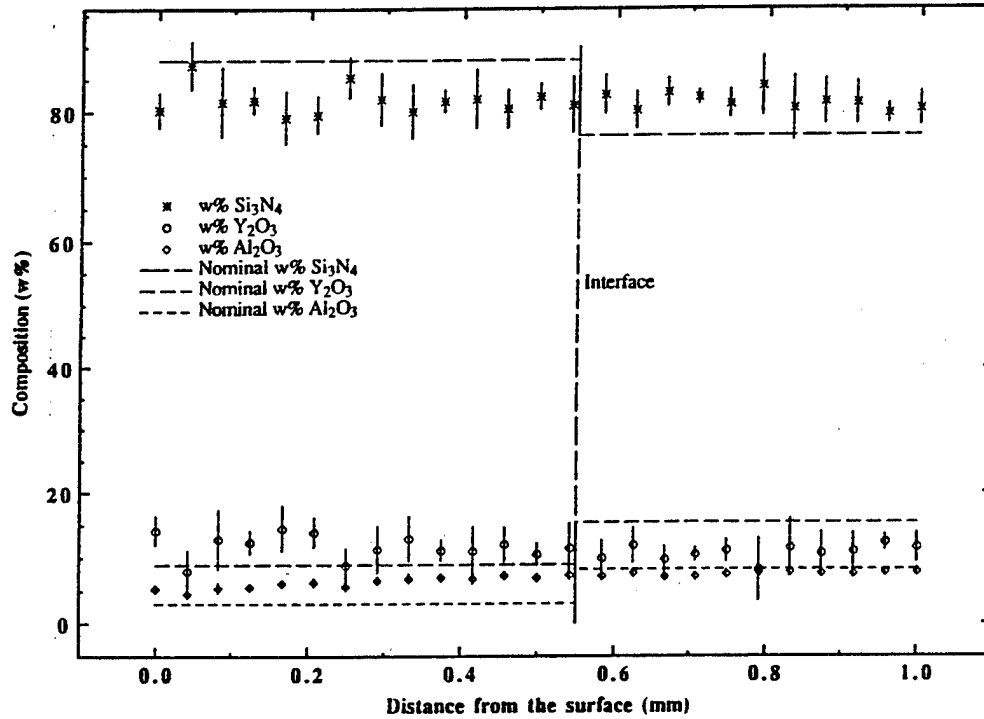


Figure 7. Composition of three-layer RC2-118B/RC2-120A/RC2-118B (see Table 2) composite as a function of distance from the surface as determined by electron microprobe.

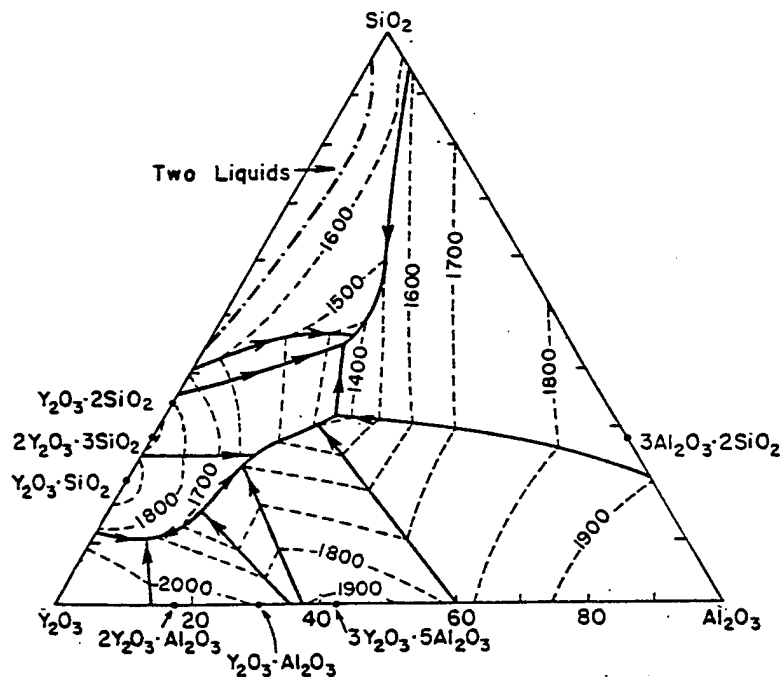


Figure 8. Phase equilibria for $\text{SiO}_2\text{-Y}_2\text{O}_3\text{-Al}_2\text{O}_3$ [45] showing liquid formation at the temperature used to sinter compositions shown in Table 2.

Table 4
Si₃N₄, Si₃N₄-TiN, SiC, and SiC-TiC Compositions

Designation	Composition (wt. %)						T.D. ^a (g/cc)	α^b (20-1200°C)
	Si ₃ N ₄ ^c	SiC ^d	Al ₂ O ₃ ^e	Y ₂ O ₃ ^f	TiN ^g	TiC ^h		
RC2-164A (outer layer)	83.00	0.00	4.00	13.00	0.00	0.00	3.38	3.6x10 ⁻⁶ /°C
RC2-164B (inner layer)	56.93	0.00	3.53	11.49	28.05	0.00	3.82	4.7x10 ⁻⁶ /°C
RC2-150A (outer layer)	0.00	95.00	2.00	3.00	0.00	0.00	3.26	5.0x10 ⁻⁶ /°C
RC2-150B (inner layer)	0.00	55.74	2.00	3.00	0.00	39.26	3.78	6.0x10 ⁻⁶ /°C

a. Theoretical density of unsintered body.

b. Measured thermal expansion coefficient between 20 and 1200°C.

c. Starck grade LC 12S

d. Lonza grade UF-15

e. Reynolds grade ERC DBM.

f. Molycorp grade 5600.

g. Starck grade C.

h. Starck grade CA.

have thermal expansion coefficients of 4.9x10⁻⁶/°C, 5.3x10⁻⁶/°C, and 5.7x10⁻⁶/°C, respectively. Table 4 lists actual compositions made and measured thermal expansions, showing good correlation between predicted and measured thermal expansion.

It was difficult to find a dispersant which produced Si₃N₄-TiN slips of similar rheology as Si₃N₄. The dispersant which worked best was 2-amino-2-methylpropanol[52] at one wt. % level (based on solids). When Si₃N₄ and Si₃N₄-15 vol. % TiN slips were made at a solids content of 36 vol. %, they displayed vastly different rheological behavior. The Si₃N₄ slip displayed Newtonian behavior (viscosity at \approx 42 mPa·s as measured with a Brookfield RV spindle #3 at speeds between 5 and 100 rpm) while the Si₃N₄-TiN slip had pronounced Bingham behavior with viscosity changing from 120 mPa·s at 5 rpm to 60 mPa·s at 100 rpm. Both slips cast and dried well as monolithics but layered rods cracked due to differential shrinkage. The reason for this was differential shrinkage between layers during drying of the composite rods.

Layered Si₃N₄/Si₃N₄-15 vol. % TiN rods were successfully slip cast, dried, and sintered without cracking. The use of a coalescing agent (glycol ether) to plasticize the acrylic binder system did not prevent cracking. However, when the solids content in the inner layer slip was decreased from 36 to 33.5 vol. %, the two-layer rods could be dried

without cracking using either acrylic or urethane binders at a level of 0.5 wt. % (based on solids). The lower solids content loading of the Si_3N_4 -TiN may have helped to minimize differential shrinkage during drying. The green density of the inner layer was lower such that the inner layer contracted more on drying, putting the outer layer under compression to eliminate cracking.

Particle size measurements (see Figure 9) showed that the outer layer slip had a median diameter of $0.5\ \mu\text{m}$ (modal diameter of $0.3\ \mu\text{m}$) while the inner layer slip had a median diameter of $0.7\ \mu\text{m}$ (modal diameter of $0.8\ \mu\text{m}$). The larger agglomerate size of the inner-layer slip is due to the coarser size of TiN relative to Si_3N_4 , as well as the difficulty in dispersing TiN.

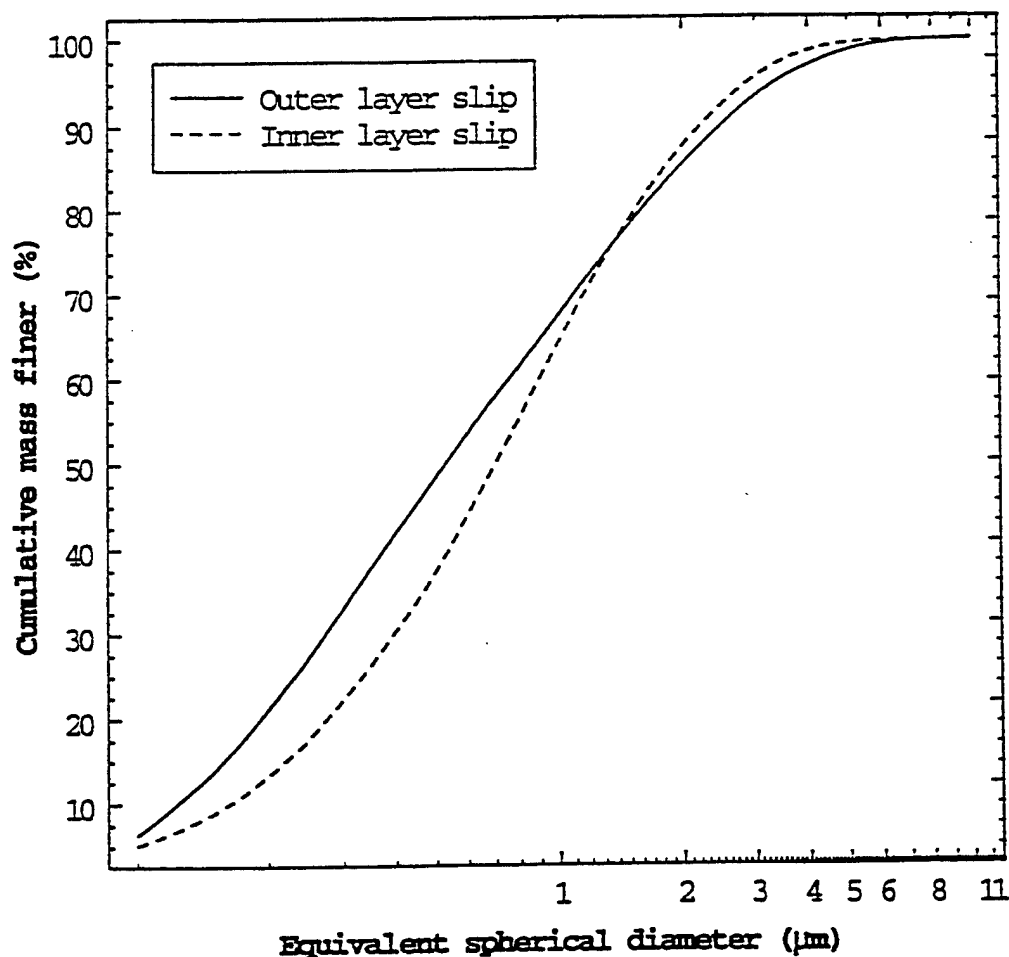


Figure 9. Agglomerate size distributions of Si_3N_4 (outer layer) and Si_3N_4 -15 vol. % TiN (inner-layer) slips dispersed using 1 wt. % 2-amino-2-methylpropanol[52] in water.

Due to the ease in dispersing both SiC and TiC simultaneously with 0.2 wt. % lignosulfonate and 0.4 wt. % NH_4OH (based on solids), SiC/SiC-TiC layered composites were easy to cast, dry, and cosinter. Comparisons of the viscosity of SiC and SiC-TiC slips with Si_3N_4 and Si_3N_4 -TiN slips are presented in Figure 10. Similar viscosities for SiC and SiC-TiC slips over a wide range of shear rates results in outer and inner layers of layered composites having similar green density, which results in near identical drying behavior. The similar sintering temperature also makes this system ideal for introducing substantial compressive stress. The relatively high creep resistance of this system allows the sintering of straight rods. This is extremely important for layered rods since distortion results in nonuniform layer thickness after grinding.

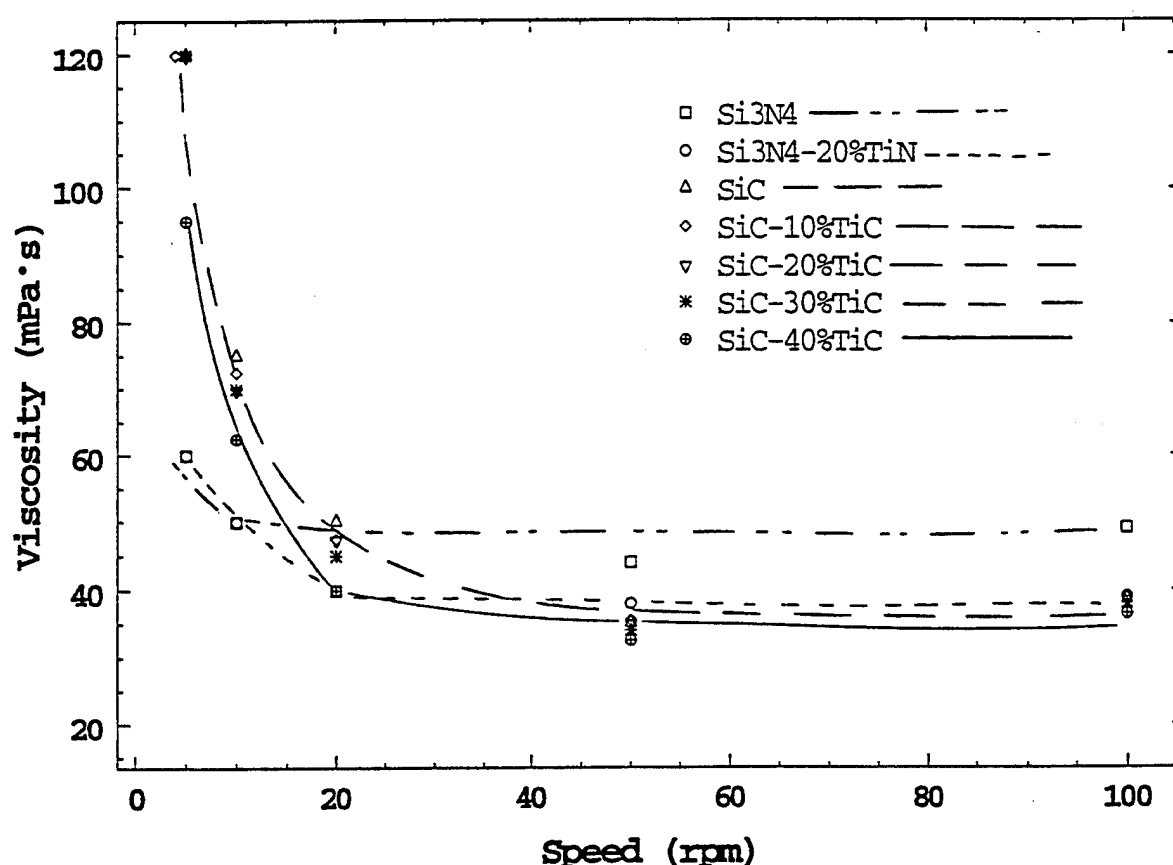


Figure 10. Viscosity comparison of Si_3N_4 -6 wt. % Y_2O_3 -2 wt. % Al_2O_3 at 35 vol. % solids with " Si_3N_4 "-20 vol. % TiN at 32.3 vol. % solids. SiC-3 wt. % Y_2O_3 -2 wt. % Al_2O_3 and "SiC" with 10, 20, 30, or 40 vol. % TiC slips at 30 vol. % solids are shown for comparison. While it was possible to disperse Si_3N_4 -based slips at higher solids loadings than SiC-based slips, the advantage of SiC and SiC-TiC slips is that they had similar viscosities at the same solids content, which reduced strain caused by shrinkage during drying.

The limitations of SiC-TiC are: 1) volatilization at high temperatures due primarily to reactions between Al_2O_3 and SiC, such as $\text{SiC} + \text{Al}_2\text{O}_3 \rightarrow \text{SiO} + \text{Al}_2\text{O} + \text{CO}$, which result in gaseous products which cause surface pitting (this is reduced by overpressure of the reaction products by sintering in a closed graphite crucible), and 2) the difficulty in achieving nearly theoretical density (T.D.). It is easy to reach closed porosity (>94% T.D.) and routine to achieve >98.5% of theoretical density, but it is very difficult without applied pressure to sinter to near 99.9% T.D.. Cundill[19] has stated that 0.1% porosity is high for bearing materials. Although high temperature HIPing has been shown to aid liquid phase sintered SiC[39,43], it is not cost effective since Si_3N_4 bearings are already made in this manner. As will be shown below, the introduction of compressive surface stresses does not eliminate spalling in liquid phase sintered SiC with $\approx 1\%$ porosity.

In summary, it was not possible to cosinter a Si_3N_4 outer layer with a SiC or SiC- Si_3N_4 even with liquid phase sintering. However, it was possible with both Si_3N_4 and SiC-based systems to cosinter layered RCF rods. The addition of TiN to Si_3N_4 and TiC to SiC are effective methods for tailoring the proper strain due to thermal expansion mismatch. Stable aqueous slips for Si_3N_4 , Si_3N_4 -TiN, SiC, and SiC-TiC suspensions were developed during this program. Both monolithic and layered plates and RCF rods were cast, dried, sintered, and prepared for characterization and RCF testing.

The requirements for a successful CVD coating are: 1) high deposition rate (>25 $\mu\text{m/hr}$) to give 200-300 μm coating, 2) good bonding at interfaces, 3) thermal expansion mismatch ($\approx 1 \times 10^{-6}/^\circ\text{C}$) to give compressive strength of 400-800 MPa, 4) moderate to high strength coating (i.e., amorphous or fine (<5 μm) grain size and low porosity in coating), and 5) thickness uniformity.

Initial expectation from CVD vendors (Astro Technologies and Ultramet) was that it would be possible to put down a 200-300 μm Si_3N_4 coating. Neither vendor could deposit amorphous Si_3N_4 at sufficient rates to generate a coating this thick. As will be shown later, typical Si_3N_4 coating thicknesses were 25-50 μm . Due to the inability of finding an economical method of depositing Si_3N_4 , it was decided to deposit CVD SiC on pressureless sintered SiC-TiC substrates.

4.2 Slip Cast and Cosintered Materials

Liquid phase sintered SiC can be made with respectable strength and reliability by slip casting as shown in Figure 11 for a SiC-2 wt. % Y_2O_3 -1.7 wt. % Al composition. The Al scavenges O to become Al_2O_3 and then reacts to form yttrium aluminates at high temperature. Table 4, above, gives the compositions of SiC (RC2-150A) and SiC-30 vol. % TiC (RC2-150B). The addition of TiC improves the ease of grinding, and layered plates

and rods were made using SiC-15 vol. % TiC (RC2-164C) as the outer layer material and SiC-30 vol. % TiC (RC2-164D) as the inner layer. The addition of TiC to SiC did not significantly affect strength, as shown in Table 5. Composition RC2-164D was a duplicate of composition RC2-150B and both showed similar strength, as expected. The wide scatter in strength values for the 164 series bars is due to surface pits not removed by grinding which resulted in variable strength. The important point is that both monolithic and layered bars had similar pits, yet the strength of the layered bars was ≈ 170 MPa higher. The thermal expansion mismatch between SiC-15 vol. % TiC and SiC-30 vol. % TiC was measured to be $4.5 \times 10^{-7}/^{\circ}\text{C}$. The expected compressive stress in the outer layer, taking a modulus of 435 GPa, Poisson's ratio of 0.2, ΔT of 1500°C , and d_2/d of 0.71 is 301 MPa. The reason why the strength of three-layer bars (164 C/D/C) was significantly lower than expected was that the majority of bars failed from the inner layer, just below the interface. Failure from this location is expected when outer and inner layers have similar strength. Strain gage (Figure 12) and indentation/strength measurements showed (see Figure 13) that the true residual stress in the outer layer of these bars was -240 to -300 MPa, as expected based on thermal expansion mismatch.

Using the data from the strain gage measurements, Figure 14 was constructed to show the residual stresses predicted for the ground two-layer rods for which RCF data is given in Figure 15. The two different outer layer moduli used in calculating stresses for Figure 14 were based on literature values (433 MPa) and measurement (492 GPa). A

Table 5
Strength Data for SiC and SiC-TiC Composites

Designation	Strength (MPa)		Weibull Modulus	Characteristic Strength
	Ceramtec	Univ. of Utah		
RC2-150A (SiC)	587 \pm 79 (6)	483 \pm 82 (22)	7.2	516
RC2-150B (SiC-30 vol. % TiC)	490 \pm 38 (6)	507 \pm 32 (22)	17.7	506
RC2-164C (SiC-15 vol. % TiC)	451 \pm 158 (6)	---	---	---
RC2-164D (SiC-30 vol. % TiC)	493 \pm 99 (6)	---	---	---
RC2-164C/D/C (Three-layer)	620 \pm 154 (6)	---	---	---

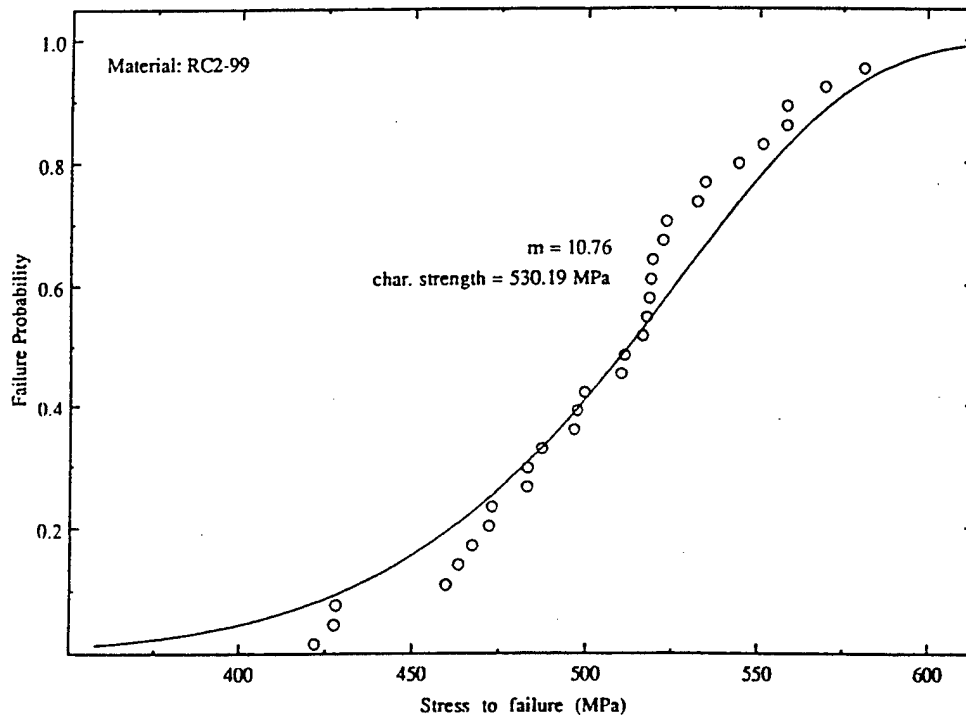


Figure 11. Weibull plot for 32 bars of liquid phase sintered SiC.

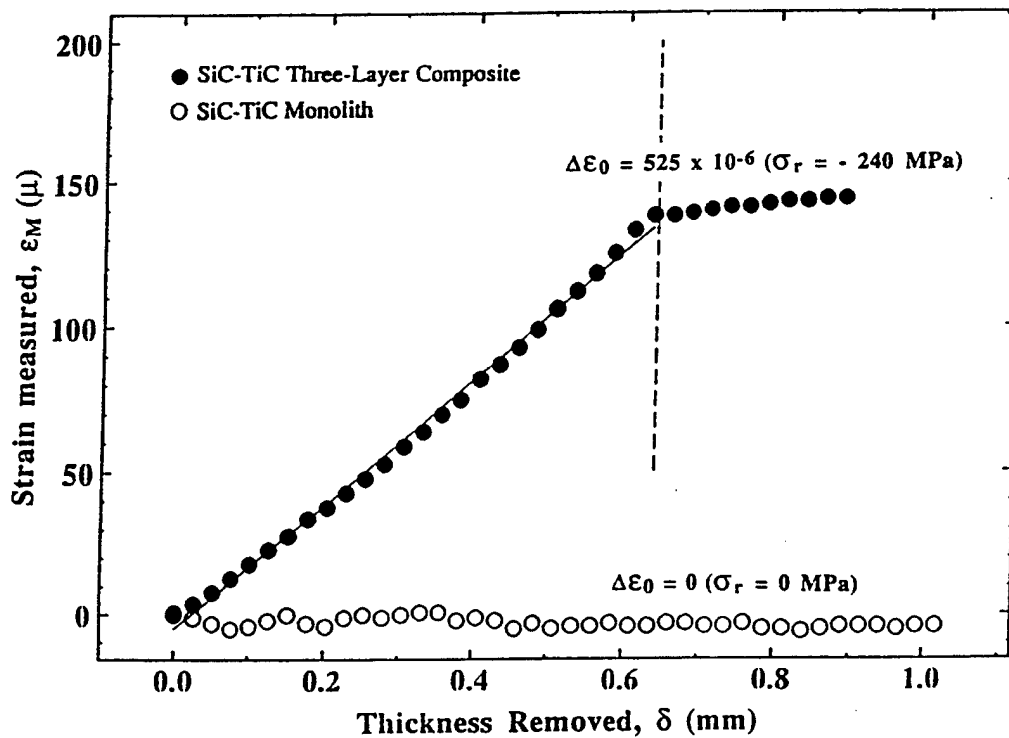
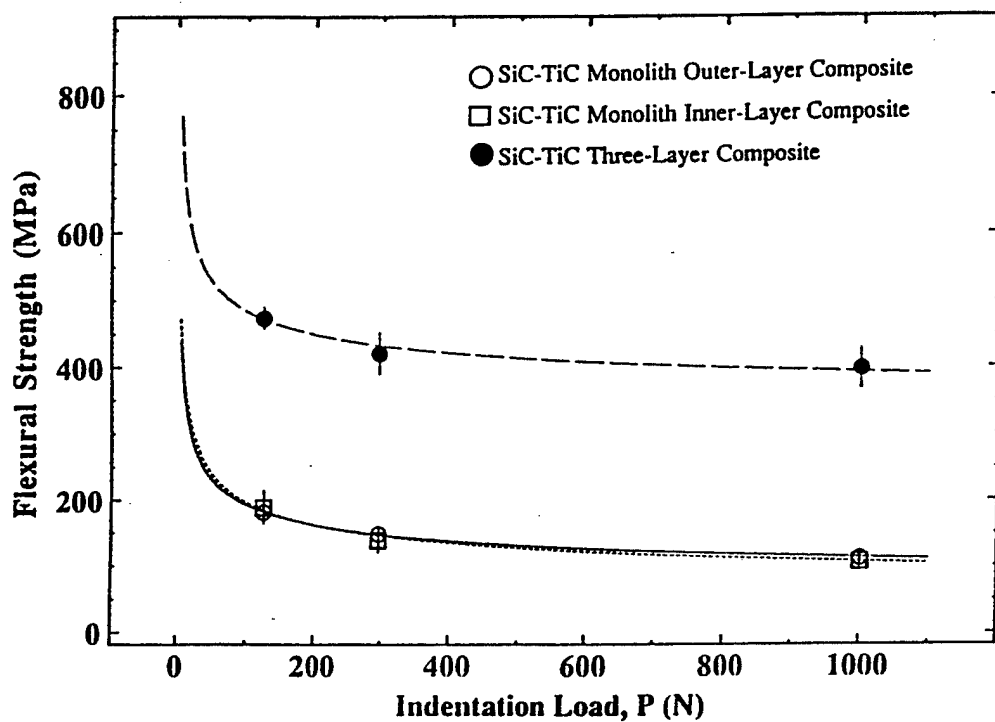
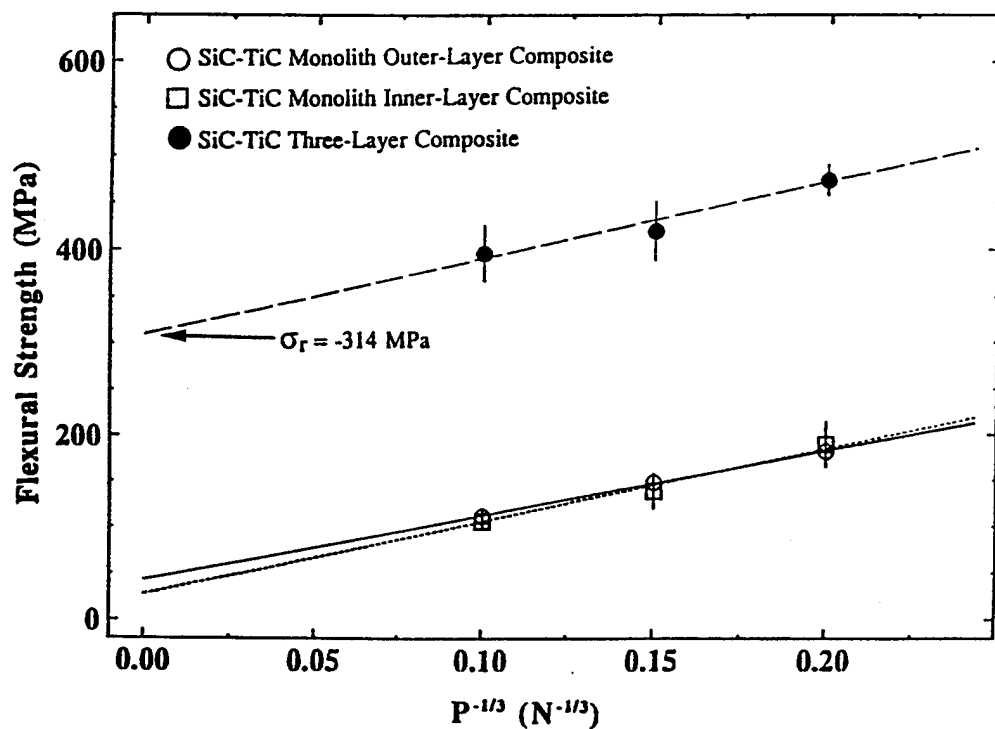


Figure 12. Strain as a function of depth of material removed for monolithic SiC-15 vol. % TiC (RC2-164C) and three-layer SiC-15 vol. % TiC/SiC-30 vol. % TiC/SiC-15 vol. % TiC (RC2-164C/D/C).

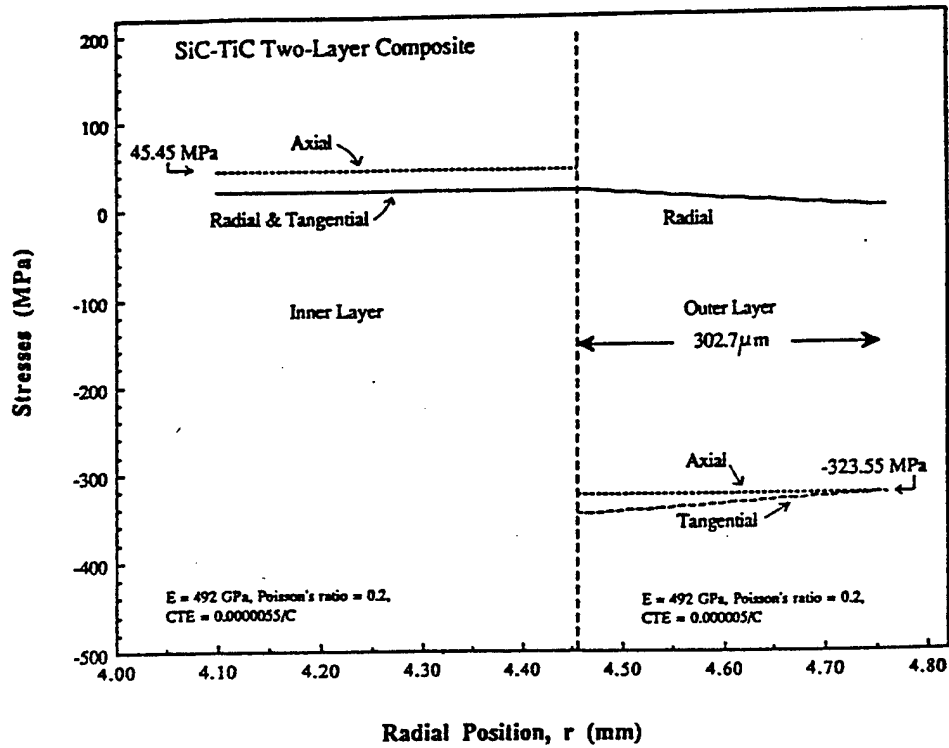


(a)

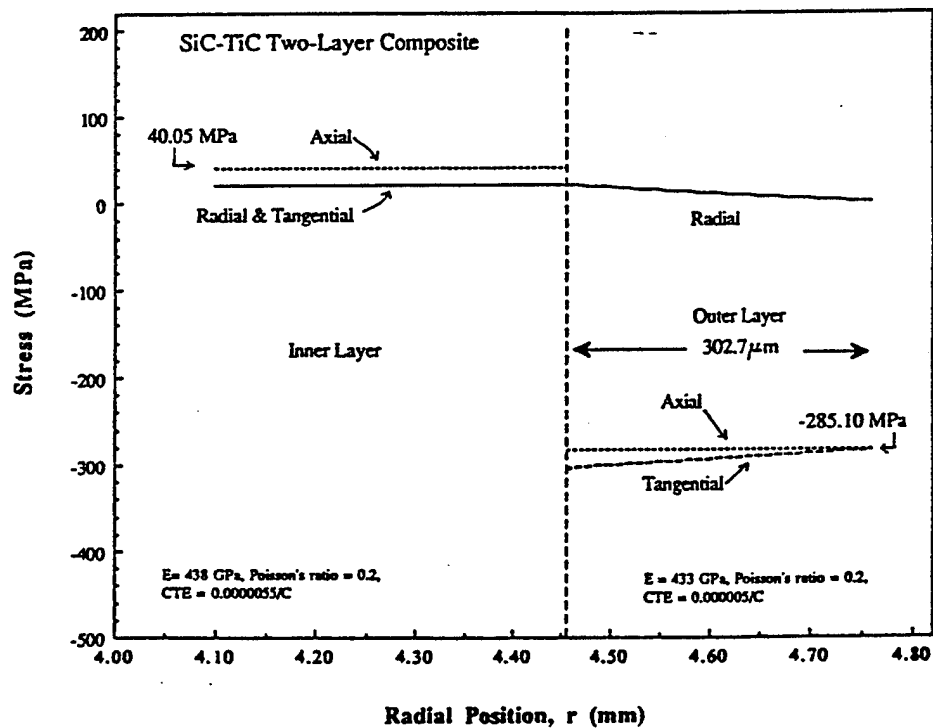


(b)

Figure 13. Flexural strength measurements as a function of: a) indentation load, P, and b) $P^{-1/3}$. Monolithic outer layer material is SiC-15 vol. % TiC, inner-layer is SiC-30 vol. % TiC, and damage resistance material is the three-layer composite.



(a)



(b)

Figure 14. Variation of radial, tangential, and axial stresses along a radius in the outer layer and part of the inner layer of two-layer SiC-15 vol. % TiC /SiC-30 vol. % TiC rod. (a) $E=492$ GPa, (b) $E=435$ GPa.

compressive stress of ≈ 300 MPa did not significantly affect the rolling contact fatigue performance of the pressureless sintered rods. While each of the data points for the layered rods lie to the right (i.e., increased lifetimes) of the corresponding datum point for the monolithic rods, they do not give the significantly higher lifetimes needed for rolling elements. SiC (RC2-150A) gave similarly short lifetimes showing that the addition of TiC to SiC was not responsible for the short fatigue lifetimes. The short lifetimes were due to rapid wear and spalling, with defects being the main failure initiation sites. The conclusion from this testing was that the introduction of substantial compressive stress (i.e., ≈ 300 MPa) did not overcome the tendency for rapid wear (due to low toughness) or spalling. The way to overcome this problem is to reduce the porosity in the liquid phase sintered SiC or to apply a CVD coating to the substrates. The latter approach is discussed under the heading of "CVD Coatings."

Si_3N_4 with 13 wt. % Y_2O_3 and 4 wt. % Al_2O_3 and " Si_3N_4 "-15 vol. % TiN were sintered as monolithic rods, as well as two-layer rods, at 1750°C for one hour. Cladless HIPing at 1750°C for 30 minutes with 220 MPa N_2 did not change the density. The thermal expansion mismatch between the outer (Si_3N_4) and the inner (Si_3N_4 -15 vol. % TiN) materials was $7.5 \times 10^{-7}/^\circ\text{C}$, resulting in residual axial and tangential stresses of ≈ 300 MPa in the outer layer (see Figure 16). RCF data for these rods are shown in Figure 17. Although the lifetime is extended with Si_3N_4 , as compared to SiC (see Figure 15), the result is the same, namely, only marginally longer lifetimes for the layered rods. Microstructural examination, as shown in Figure 18, revealed that microstructural defects caused by poor packing of the slip were the main sites of failure initiation. The fatigue spalls were similar to those experienced for Si_3N_4 during its development in the 1970s. One interesting observation, however, is that while the layered composites still spalled, the cracking within the spall was much different (see Figure 19) in that the surface compression held the fractured ceramic in place.

The key to making good silicon nitride is therefore to reduce microstructural defects. This was accomplished by lowering the additive content and sinter/HIPing. Monolithic Si_3N_4 -6 wt. % Y_2O_3 -2 wt. % Al_2O_3 and " Si_3N_4 "-20 vol. % TiN samples were bisqued at 1200°C prior to sinter/HIPing by heating from 20°C to 1750°C at $1000^\circ\text{C}/\text{hour}$ keeping the N_2 pressure below 14 MPa, holding for 15 minutes, then increasing the N_2 pressure to 200 MPa while heating to 1900°C and holding for 30 minutes. These materials had densities greater than 99.5% of theoretical density, with compressive stress of ≈ 600 MPa range (see Figure 20). RCF testing of these rods showed that both monolithic and layered rods showed no fatigue spalling at 5.5 GPa. Less expensive materials than Si_3N_4 , but with similar fatigue lifetimes, are needed to promote the use of ceramic bearings.

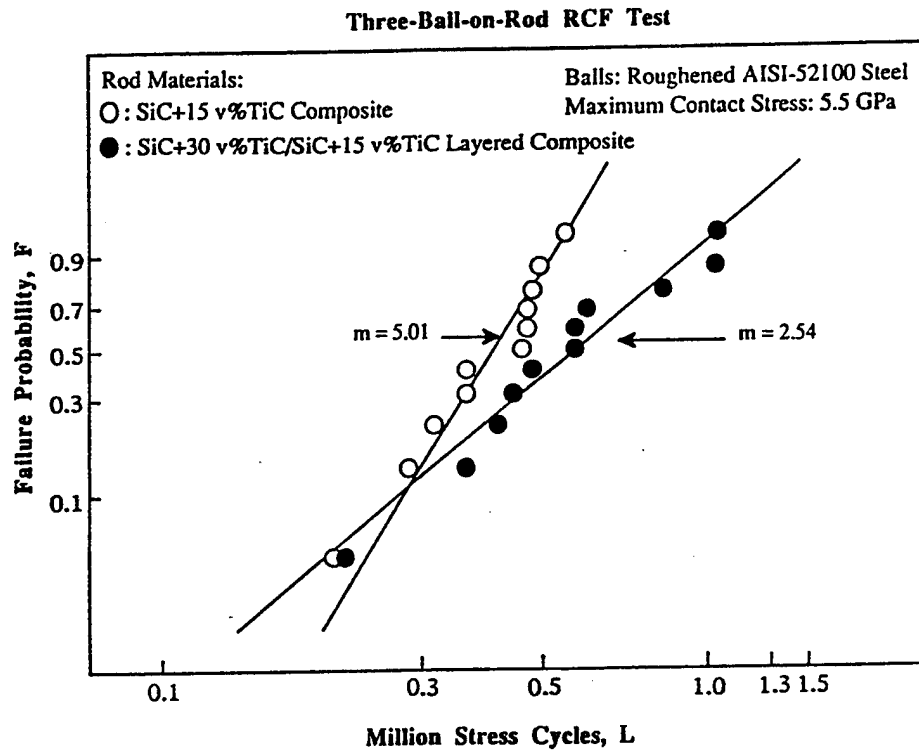


Figure 15. Weibull plots for monolithic outer layer SiC-15 vol. % TiC and two-layer SiC-15 vol. % TiC/SiC-30 vol. % TiC rods loaded initially at 5.5 GPa. Note that all data points for layered rods lie to the right of monolithic rod data points.

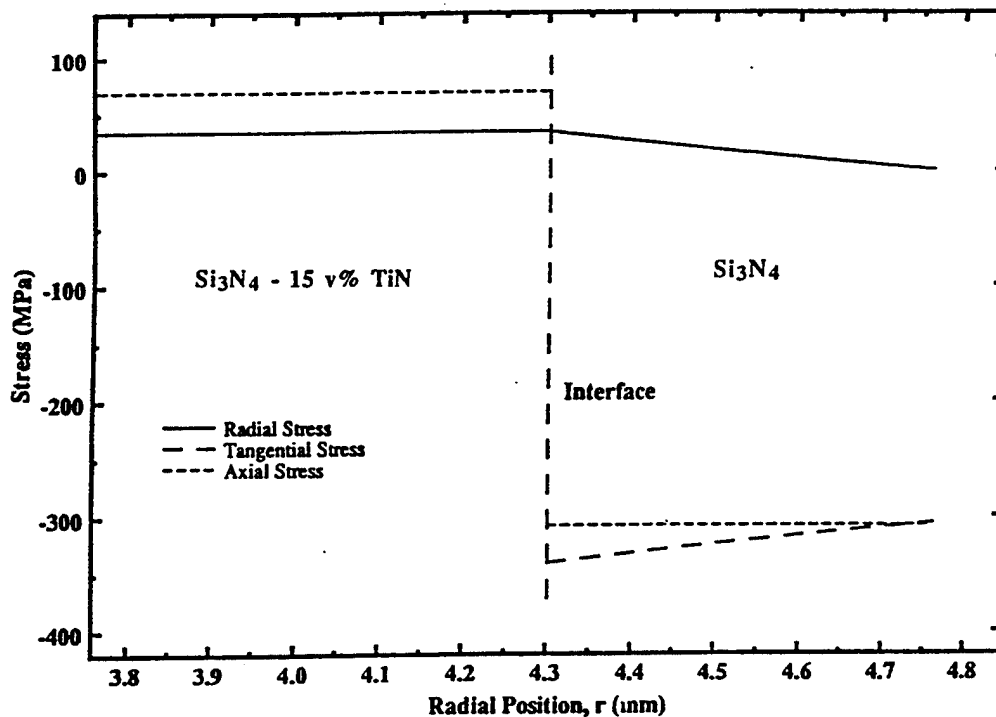


Figure 16. Variation of radial, tangential, and axial stresses along a radius in the outer layer and part of the inner layer of two-layer Si₃N₄/Si₃N₄-15 vol. % TiN rod.

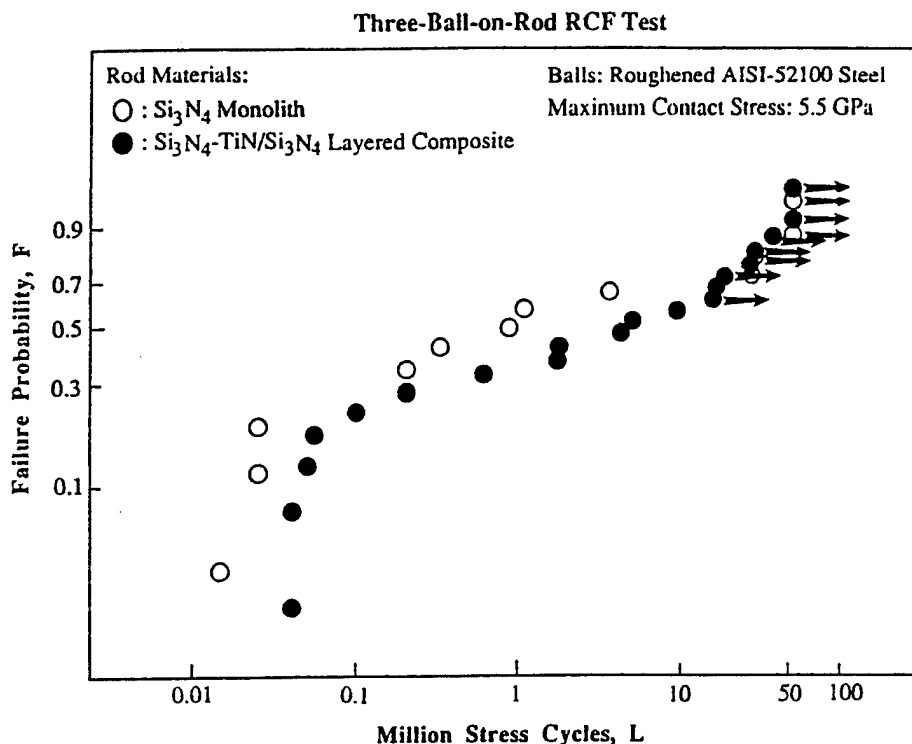


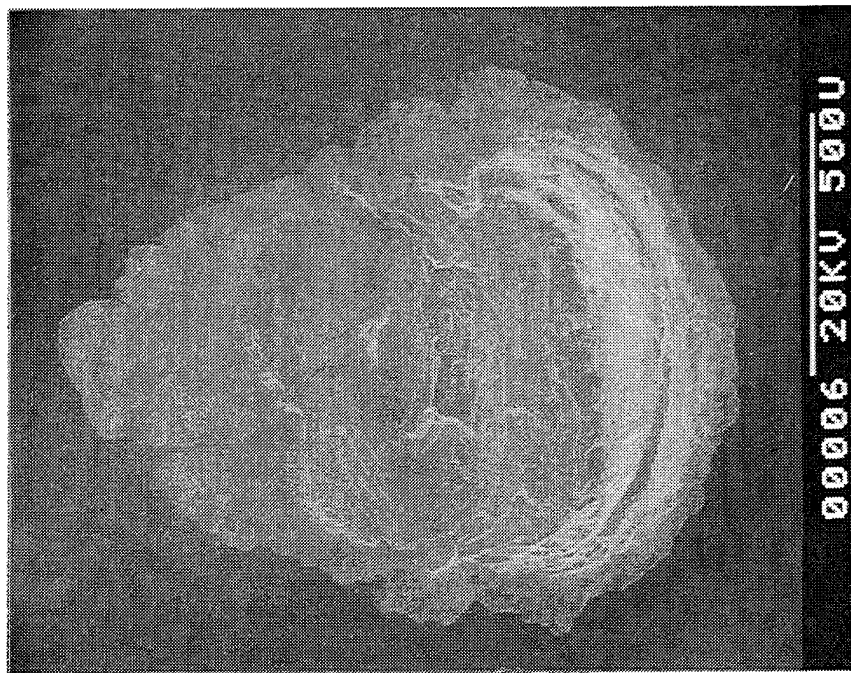
Figure 17. Weibull plots for monolithic outer layer Si_3N_4 and two-layer $\text{Si}_3\text{N}_4/\text{Si}_3\text{N}_4\text{-15 vol. \% TiN}$ rods loaded initially at 5.5 GPa. Note that layered rods show minimal improvement in RCF lifetimes (i.e., as compared to monolithic rods).

The expectation for slip casting and cosintering was that it could be less expensive than the present method of glass-encapsulated or cladless HIPing of Si_3N_4 due to the following reasons: 1) compressive stresses would eliminate the need for HIPing, 2) liquid phase sintered SiC is easy to process and uses inexpensive powders, and 3) slip casting (for rods) and dip coating (for balls) are inexpensive techniques. These expectations were not met since HIPing is needed to eliminate voids which initiate spalling and variable outer layer thickness on layered rods occurs in Si_3N_4 due to distortion during sintering. While it was possible to fabricate and test slip cast, cosintered rods, no significant performance advantages or cost-savings were realized. This technique should not be pursued for rolling bearing elements.

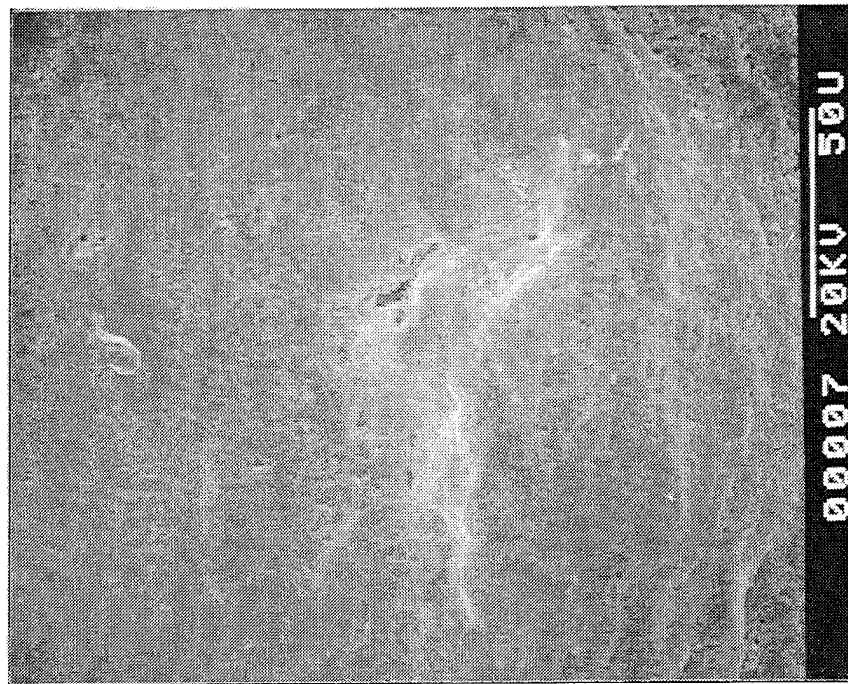
4.3 CVD Coatings

Applying Si_3N_4 by vapor deposition was slow as noted above. Table 6 compares the thickness of Si_3N_4 coatings on various substrates using SEM and optical techniques. The small coating thicknesses (<35 μm in all cases) resulted despite coating for 10 hours at 1000°C by Astro Technologies. The strength degradation of the coated Si_3N_4 was caused by an increase in the surface roughness due to uneven coating of the substrates and the use of a graded SiC- Si_3N_4 coating, where the higher expansion initial SiC coating put the Si_3N_4 in tension.

ROLLING-CONTACT FATIGUE SPALL ON MONOLITHIC Si_3N_4



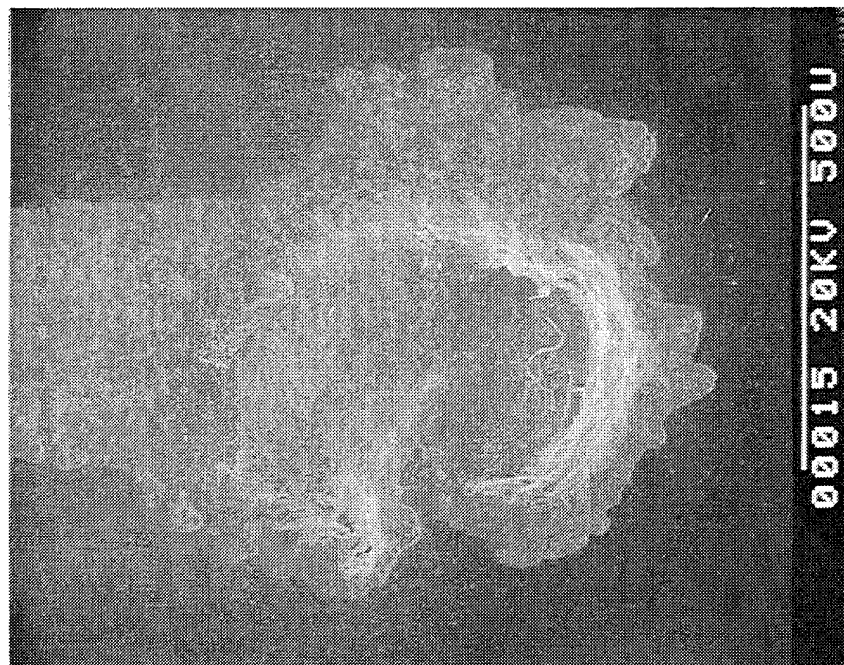
Spall (L = 0.03 Million Cycles)



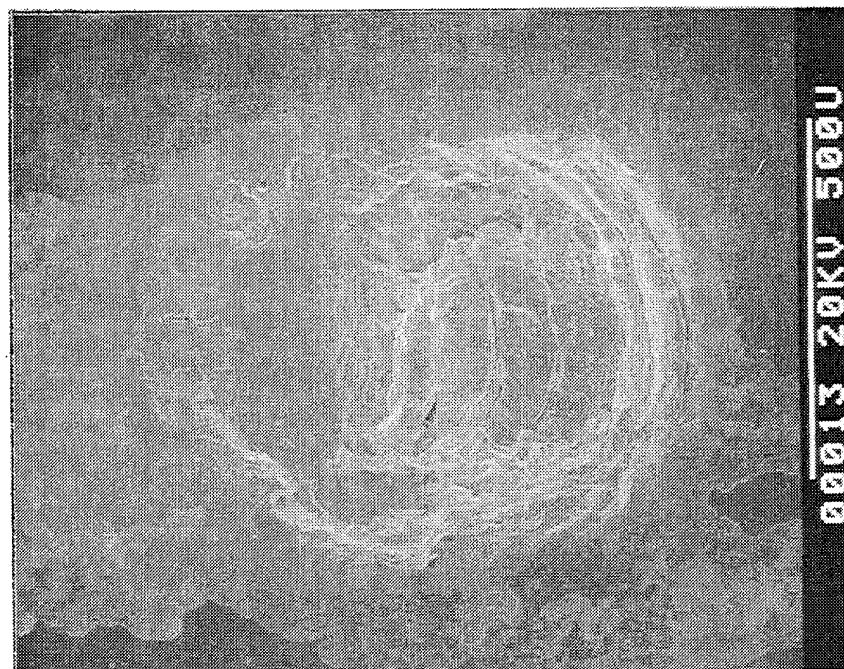
Microstructural Defect

Figure 18. Microstructure of monolithic Si_3N_4 rods tested in rolling contact fatigue at 5.5 GPa showing spall and fracture initiation site.

ROLLING-CONTACT FATIGUE SPALLS ON SILICON NITRIDE



Monolithic Si₃N₄
(L = 1.08 Million Cycles)



Layered Si₃N₄-TiN/Si₃N₄ Composite
(L = 1.75 Million Cycles)

Figure 19. Microstructure of monolithic Si₃N₄ (left) and layered Si₃N₄-15 vol. % TiN (right) rods tested in rolling contact fatigue at 5.5 GPa showing spall and fracture initiation site.

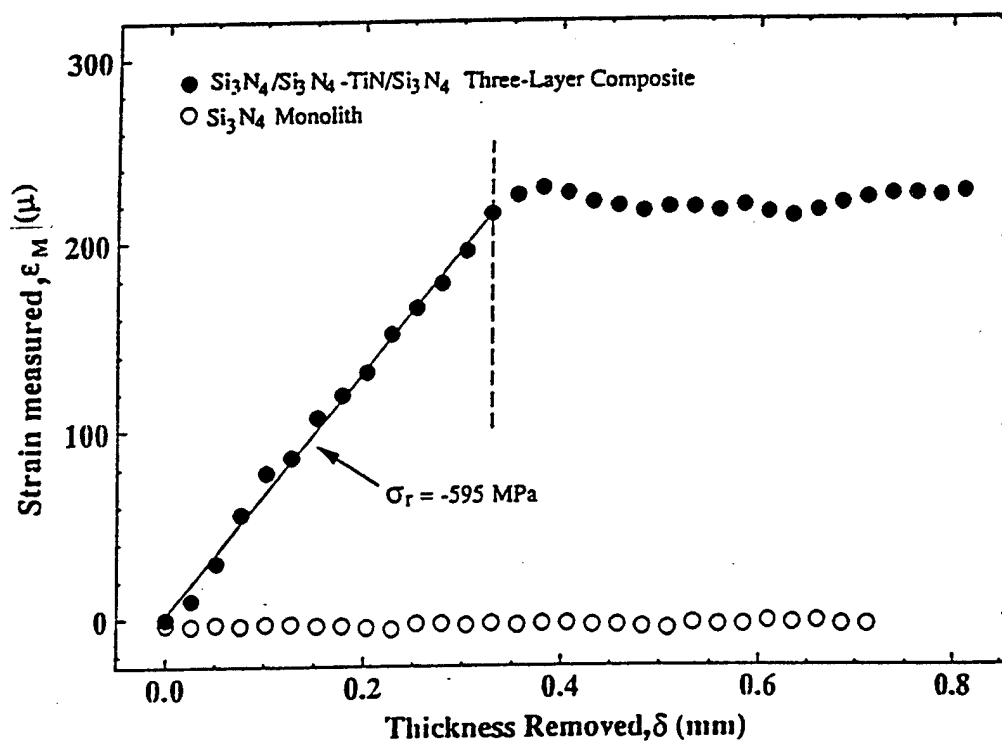


Figure 20. Strain as a function of depth of material removed for monolithic Si_3N_4 and three-layer $\text{Si}_3\text{N}_4/\text{Si}_3\text{N}_4$ -20 vol. % $\text{TiN}/\text{Si}_3\text{N}_4$.

Table 6
Thickness and Strength of CVD Si_3N_4 Deposited at 1000°C for 10 Hours

Designation (Composition)	$\alpha(10^{-6}/^\circ\text{C})$ (20-1200°C)	Coating Thickness (μm)		Bend Strength (MPa)	
		SEM	Optical	Uncoated	Coated
RC1-128A (SiC-2.5 vol. % YAG)	5.0	1-6	2-4	365±61	381±40
RC1-128B (SiC-2.5 vol. % YAG)	4.9	5-13	4-8	322±39	340±58
RC1-136A (SiC-5 vol. % YAG)	5.0	---	1-4	396±37	416±14
X188 (SiC-10 vol. % YAG)	5.1	6-21	6-11	309±24	331±25
NT 154 (Norton Si_3N_4)	3.3	9-25	12-17	902±72	281±34
95-5 (Si_3N_4 -5 vol. % $3\text{Al}_2\text{O}_3\cdot 2\text{SiO}_2$)	3.3	19-34	17-30	472±44	342±51
30-70 ($3\text{Al}_2\text{O}_3\cdot 2\text{SiO}_2$ -30 vol. % Si_3N_4)	4.8	15-19	16-23	363±51	310±85

A second coating experiment was performed at Astro Technologies with similar conditions as the first experiment except that the coating time was increased from 10 to 17 hours. No intermediate SiC layer was used and the bars were positioned horizontally rather than vertically in the CVD chamber. Table 7 gives the coating thickness for both sides of the bar, as well as the predicted residual stresses in the bars. As can be generally seen, the coating was thicker on the upward facing side of the bar than the downward facing side, as expected. The coating uniformity was generally good but the deposition rate was lower than predicted and consequently the coating thickness was much lower than the desired 200-300 μm thickness. Consequently, the bars could not be ground to produce the same surface as the uncoated bars for strength testing. Figure 21 shows the strength comparison between uncoated and coated bars of SiC-4 vol. % YAG. Due to the rougher surface of the CVD coated bars, no valid comparison could be made. Assuming a three-layer geometry with equal thickness outer layers (same as the tension face in Table 7) and that the amorphous Si_3N_4 coating has a thermal expansion of $3.0 \times 10^{-6}/^\circ\text{C}$, the calculated compressive stress in the outer layers and corresponding tensile stress in the inner layer are given in Table 7. The tensile stress in the materials is low and will not initiate failure upon cooling. Surprisingly, the SiC with the highest compressive stress appeared to be the best bonded of any of the materials. Similar bars were sent to a second vendor, Ultramet, who could not even adhere their Si_3N_4 to any of the compositions.

Table 7
Thickness and Residual Stresses Resulting From CVD Si_3N_4 Deposited at 1000°C for 17 Hours

Designation (Composition)	α (20-1200°C)	Coating Thickness (μm)		Residual Stress (MPa)	
		Tension ^a	Compression ^b	Coating	Substrate
RC2-129A (Si_3N_4 -13 wt.% Y_2O_3 -4 wt.% Al_2O_3)	3.9	25.5 \pm 6.2	0.0 \pm 0.0	-351	6
RC2-118B (Si_3N_4 -9 wt.% Y_2O_3 -3 wt.% Al_2O_3)	4.2	14.5 \pm 11.6	1.7 \pm 1.5	-495	5
RC2-118A (RC2-118B+10 vol. % YAG)	4.3	57.8 \pm 10.9	11.7 \pm 6.9	-502	18
RC2-129B (RC2-129B+10 vol. % TiN)	4.5	13.5 \pm 5.3	1.7 \pm 1.5	-599	5
RC2-99A (SiC-2 wt. % Y_2O_3 -1.7 wt. % Al)	5.1	25.3 \pm 6.5	32.6 \pm 4.8	-875	14

a. Side of bar loaded in tension during strength testing.

b. Side of bar loaded in compression during strength testing.

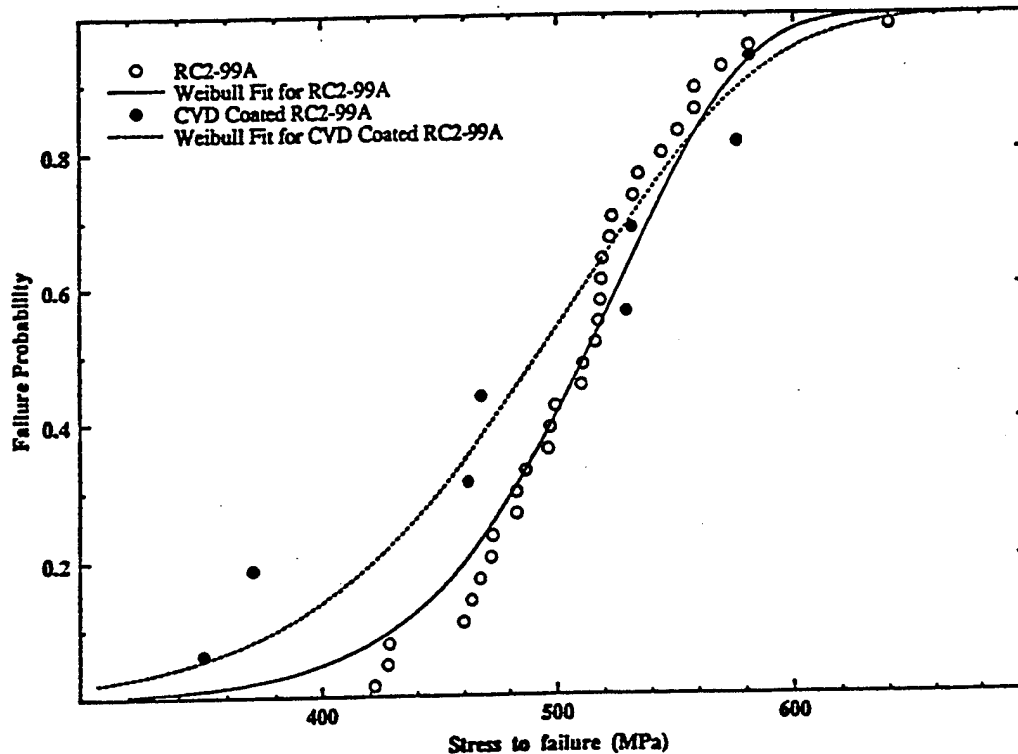


Figure 21. Weibull plots for Si_3N_4 coated ($<20 \mu\text{m}$ coating) SiC as compared with ground SiC of the same composition. The surface finish of the coated bars is inferior to the uncoated bars.

While it is possible that there is a vendor who can put down a 200-300 μm Si_3N_4 coating, it is clear that such coatings would be prohibitively expensive due to low deposition rates. Further CVD efforts were directed at SiC since it is used to coat graphite at rates up to 0.3 $\mu\text{m}/\text{minute}$ on an industrial scale and large scale reactors are available. Du Pont Lanxide provided the CVD coating discussed below, at no cost to the program.

Du Pont Lanxide coated SiC-15 vol. % TiC strength bars with a uniform ($\approx 60 \mu\text{m}$) coating of SiC by placing the bars in a 1000°C cycle used for chemical vapor infiltration (CVI). Although the coating was thinner than desired, it was uniform and dense and six coated and six uncoated bars were tested under identical conditions. The uncoated bars had a strength of $371 \pm 25 \text{ MPa}$ while the coated bars had a strength of $408 \pm 21 \text{ MPa}$. While the typical pore size in the uncoated material was less than $5 \mu\text{m}$, fractures initiated due to large defects in the substrate material. Similar defects were seen in the monolithic material such that none of the failures occurred due to grinding flaws. The residual stresses were calculated to be -280 MPa and 9 MPa for the outer and inner layers, respectively. Assuming failure from just inside the interface, the load was reduced by 3% compared to that at the surface. One would therefore expect an increase in strength of at least 11 MPa

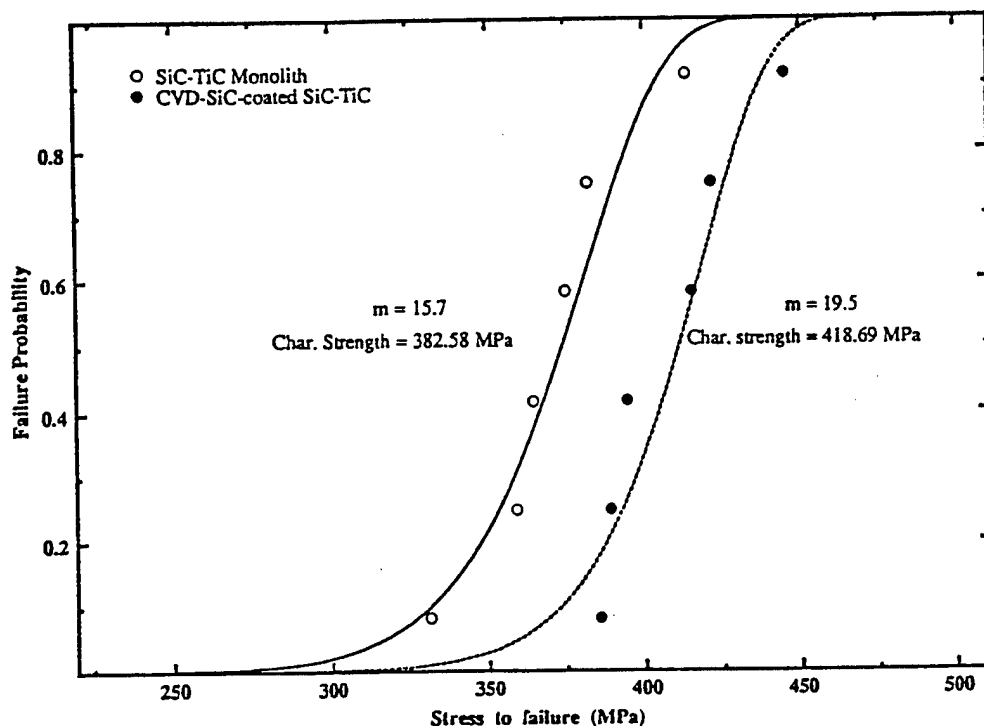


Figure 22. Weibull plots for SiC coated ($\approx 60 \mu\text{m}$ coating) and uncoated SiC-15 vol. % TiC with identical surface finish. All fractures initiated from processing flaws in the SiC-15 vol. % TiC slip cast material. Processing flaws were due to binder burnout.

due to the internal fracture initiation and a corresponding decrease in strength of 9 MPa due to the tensile residual stress in the inner layer. The fact that the two strength distributions overlap within one standard deviation is therefore consistent with expectation.

RCF rods of SiC and SiC-30 vol. % TiC (see RC2-150A and RC2-150B in Table 4) were ground 400 μm undersize on their diameter and coated using the same CVI process by Du Pont Lanxide. Due to the slow deposition times used in their CVI process, the coated rods were cooled to room temperature twice, reheated, and the CVI process was continued until the coating thickness exceeded 250 μm . The coated rods were ground in a similar manner to the RCF Si_3N_4 rods tested previously (see Fig. 15 and 17).

An interesting observation during the course of surface finishing the RCF rods was the relative roughness of the CVD-SiC surfaces as compared to a commercial-grade Si_3N_4 , as shown in Figure 23. With the same grinding procedure described above, the CVD SiC surfaces finished to a much finer surface finish (arithmetic average roughness, $R_A = 0.028 \mu\text{m}$) than did the Si_3N_4 rods ($R_A = 0.175 \mu\text{m}$). This result points to a possible cost saving in surface finishing of CVD-SiC bearing elements as compared to Si_3N_4 .

Figure 24 shows strain gage data from CVD SiC/SiC/CVD SiC and CVD SiC/SiC-30 vol. % TiC/CVD SiC bars coated in the same cycle. Figure 25 uses the strain gage data

Profilometer Traces From As-Ground Surfaces

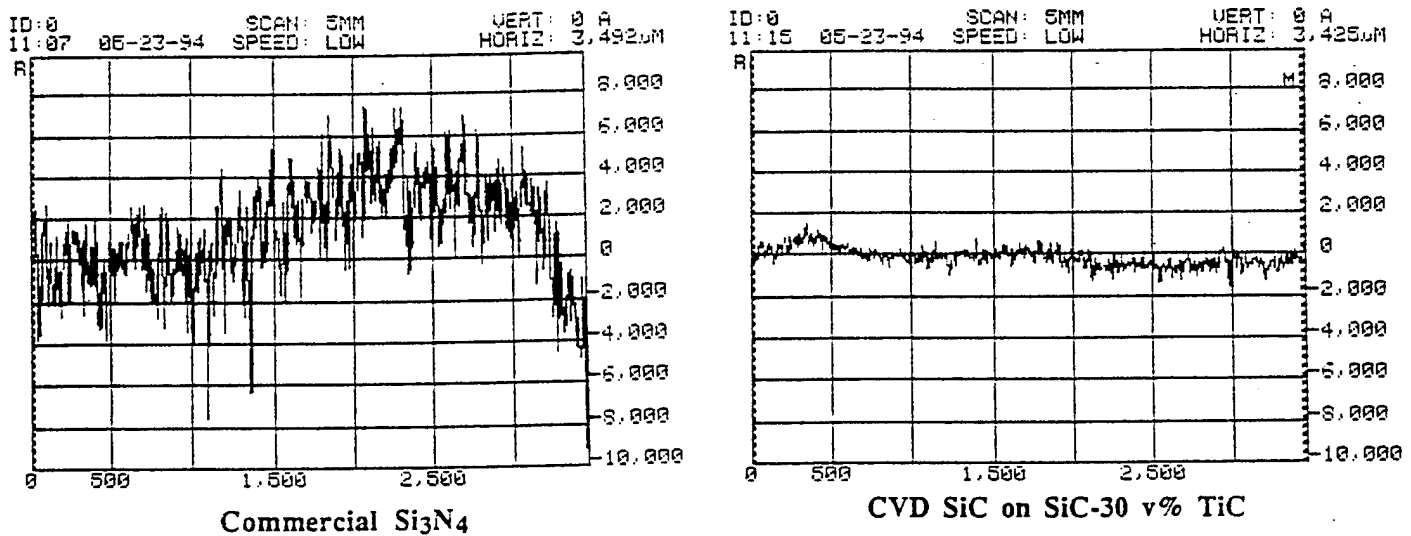


Figure 23. Surface finish comparison between CVD SiC and a commercial Si₃N₄ bearing material finished to the same specifications by the same vendor. Note the better surface finish for CVD SiC.

to predict the stresses in the rods coated in the same cycle. The thermal expansion mismatch between the CVD SiC coating[53] and the substrates was $\approx 3.5 \times 10^{-7}/^{\circ}\text{C}$ for the SiC substrate and $1.3 \times 10^{-6}/^{\circ}\text{C}$ for the SiC-30 vol. % TiC substrate, resulting in residual compression of ≈ 140 MPa for CVD SiC/SiC and ≈ 680 MPa for CVD SiC/SiC-30 vol. % TiC two-layer rods.

Figure 26 compares the rolling-contact fatigue lives of three types of SiC rods: monolithic SiC-15 vol. % TiC, layered CVD SiC/SiC, and layered CVD SiC/SiC-30 vol. % TiC at an initial Hertzian contact stress of 5.5 GPa. The surface compression on the three types of rods were 0, 140, and 680 MPa, respectively. Also shown on the figure is the Weibull line of RCF life for M-50 steel rods. For all the four test series, roughened steel (AISI 52100) balls and a synthetic turbo oil[§] lubricant were used. The data points with the arrows indicate either the tests suspended at an arbitrarily selected test period of 100 hours or tests suspended because of ball failures. Figure 26 shows that the CVD-SiC

[§] Exxon Turbo Oil Grade ETO 2380.

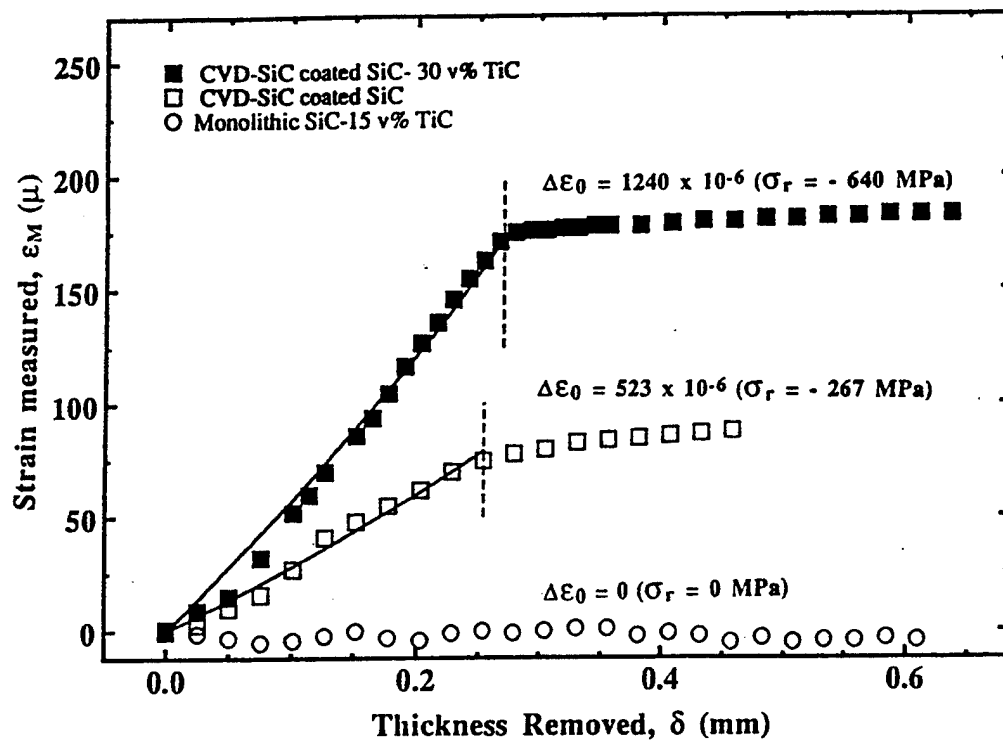


Figure 24. Strain as a function of depth of material removed for monolithic SiC-15 vol. % TiC, CVD SiC/SiC/CVD SiC, and CVD SiC/SiC-30 vol. % TiC/CVD SiC. Note that strain gage technique[1] gives clear indication of residual stress and location of interface.

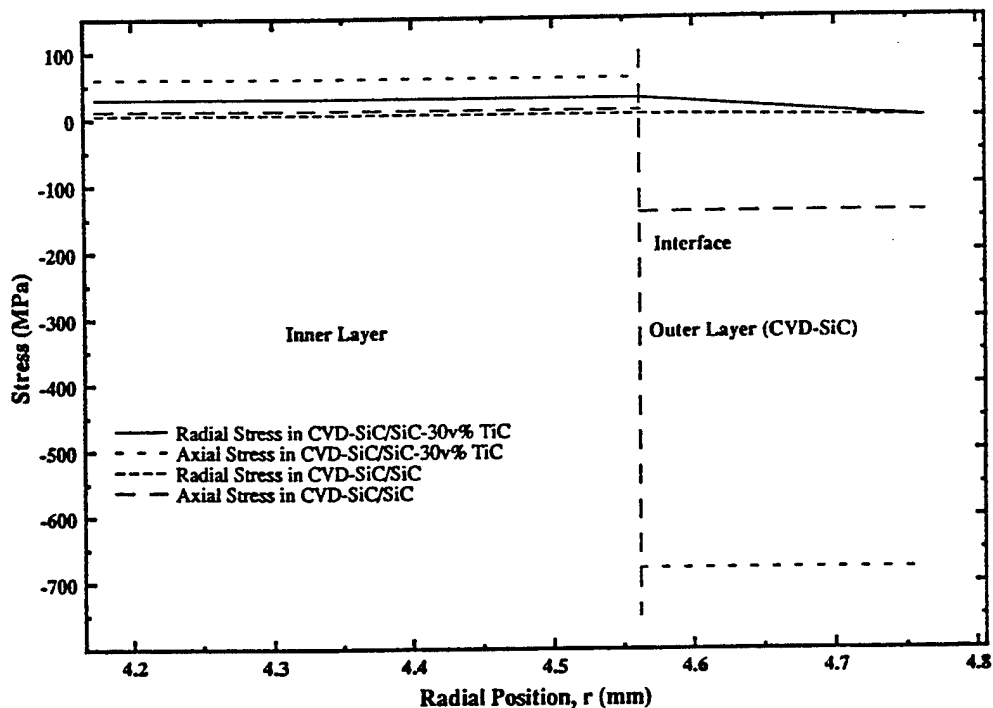


Figure 25. Variation of radial and axial stresses along a radius in the outer layer and part of the inner layer of two-layer CVD SiC/SiC and two-layer CVD SiC/SiC-30 vol. % TiC rod. Note the compressive stress difference in the outer CVD layers, which are otherwise identical.

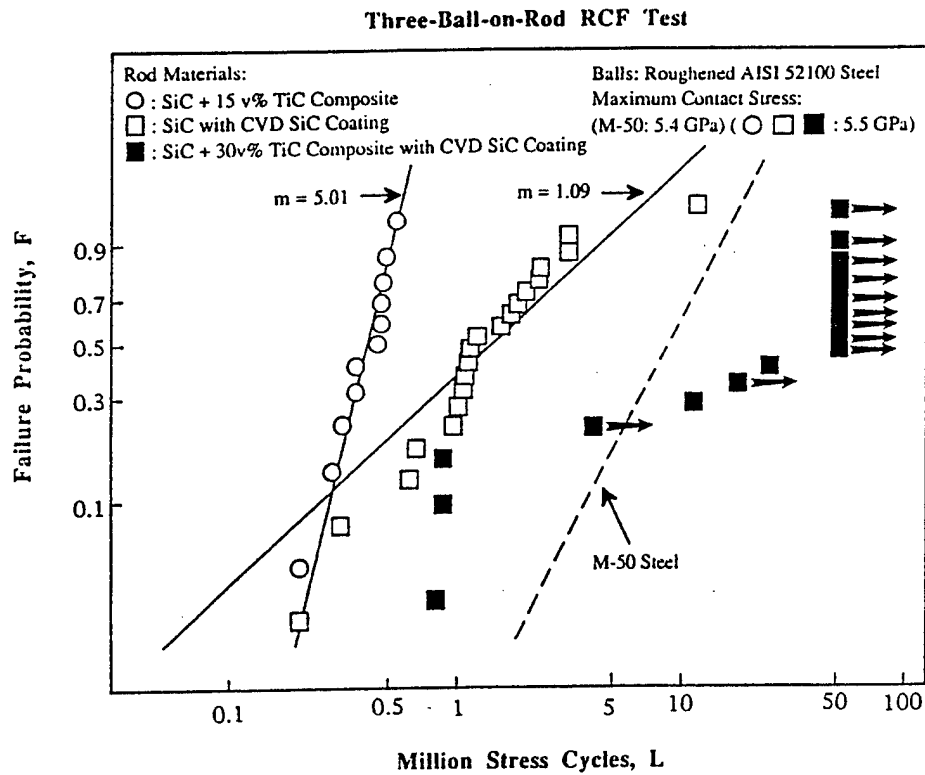
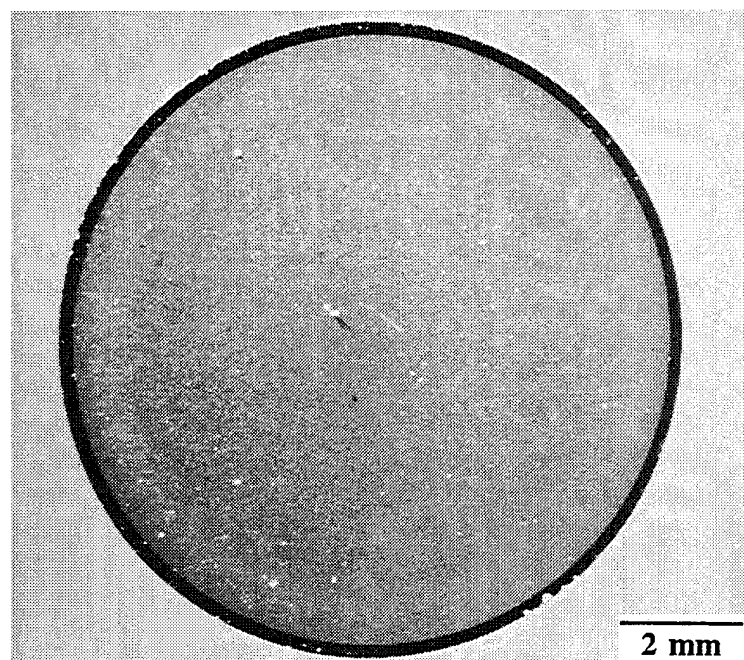


Figure 26. Weibull plots of rolling-contact fatigue lives for monolithic SiC-15 vol. % TiC (open circles), layered CVD SiC/SiC (open squares) and layered CVD SiC/SiC-30 vol. % TiC (solid squares). The monolithic SiC-15 vol. % TiC had no measurable residual stress while the surface stresses in the CVD SiC were ≈ 140 MPa for CVD SiC/SiC and ≈ 680 MPa for CVD SiC/SiC-30 vol. % TiC.

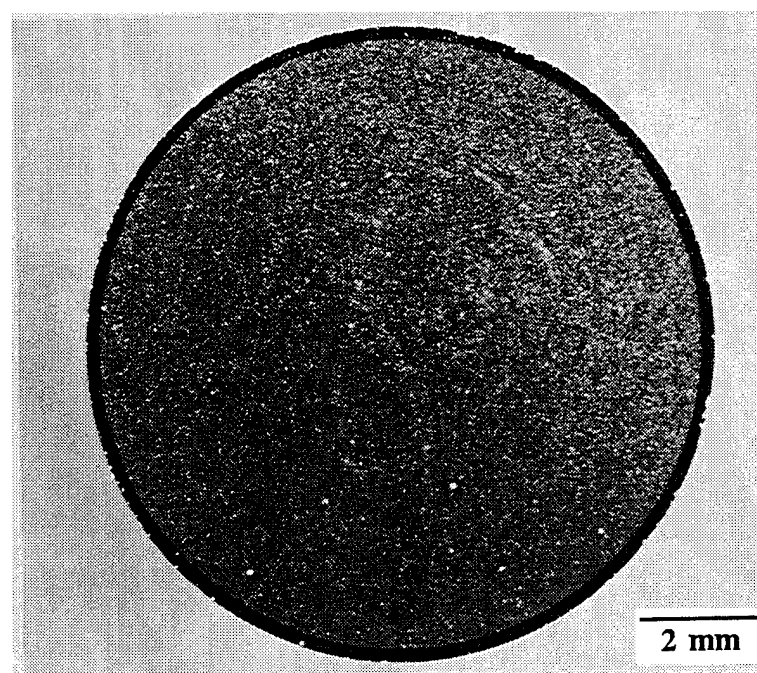
coated rods showed significantly longer life times as compared to the monolithic liquid-phase sintered SiC-15 vol. % TiC rods. Furthermore, a large fraction (9 out of 16) of the CVD-SiC coated rods with the high surface compression survived the 100 hour tests without cracking, spalling, or measurable wear.

The significance of the data displayed in Figure 26 is that a moderately high residual compressive surface stress increases the rolling contact fatigue lifetimes for ceramics, as postulated by Baumgartner in 1977[3]. The fact that dense SiC without compressive surface stresses does not have high enough toughness to avoid fracturing at similar contact stresses was demonstrated with hot pressed SiC[3]. The data in Figure 26 are believed to be the first results which show that SiC can be used as a bearing material.

The magnitude of compressive stresses in the outer layers is the only significant difference between the two SiC outer layers, since both were coated in the same Du Pont/Lanxide coating cycles. Since the samples were coated along with other samples, the cycles were interrupted two times and restarted before the desired thickness was obtained. No interface was observed on polished cross-sections (see Figure 27) until the materials were etched with Murakami's etchant. The top SEM photograph of Figure 28 shows the

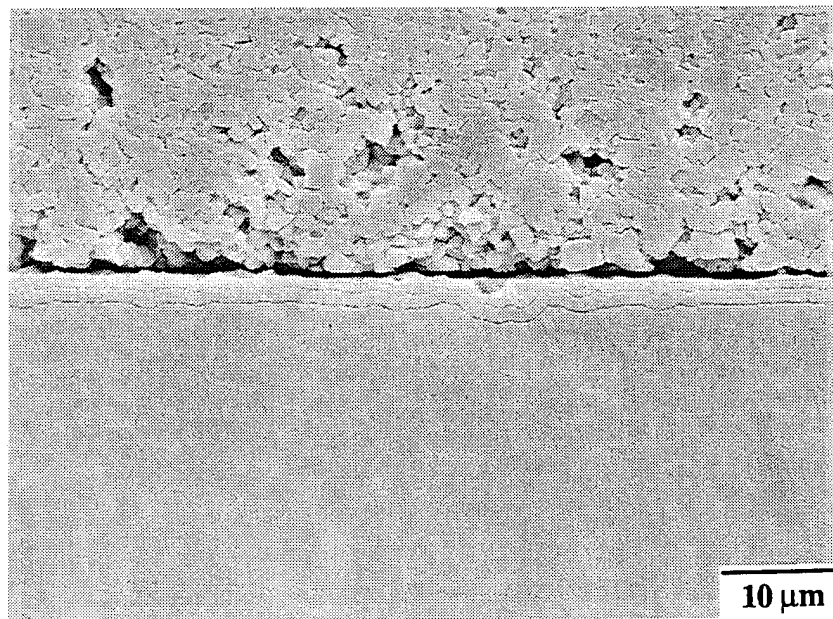


(a)

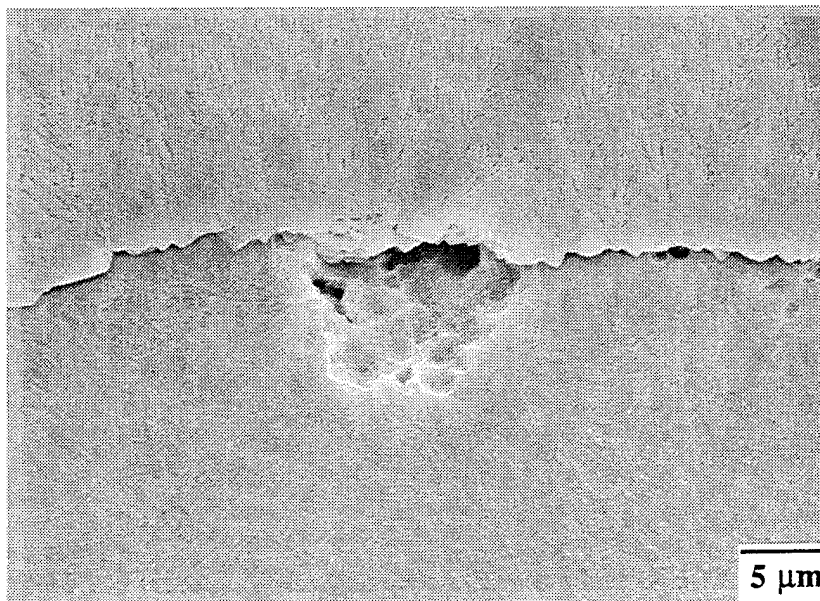


(b)

Figure 27. Optical micrographs of cross-sections of CVD SiC coated on RCF rods. (a) CVD SiC on SiC substrate, (b) CVD SiC on SiC-30 vol. % TiC substrate. Note excellent uniformity of 200 μ m SiC coating.



(a)



(b)

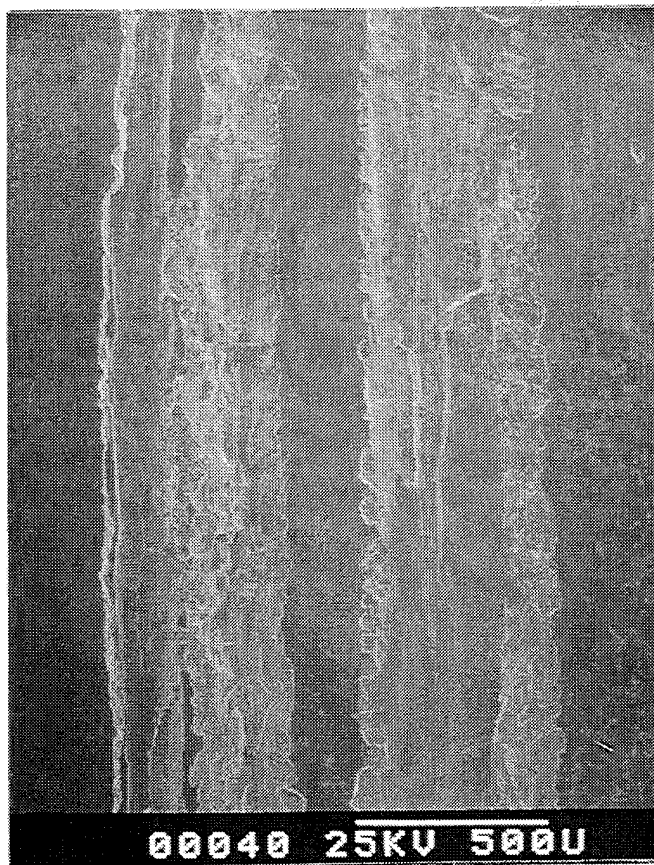
Figure 28. SEM micrographs of polished and etched CVD SiC/SiC. (a) Interface between the SiC substrate and the CVD SiC coating, (b) An interface within the CVD SiC coating caused by process interruption.

CVD SiC/SiC interface where nodular SiC growth is evident. The bottom photograph in Figure 28 shows an interface believed to be due to process interruption. This interface is located $\approx 150\text{ }\mu\text{m}$ into the $200\text{ }\mu\text{m}$ coating. The voids observed after etching were apparently filled with Si during the coating process. Neither these Si inclusions nor the process interruption were failure sites during RCF testing.

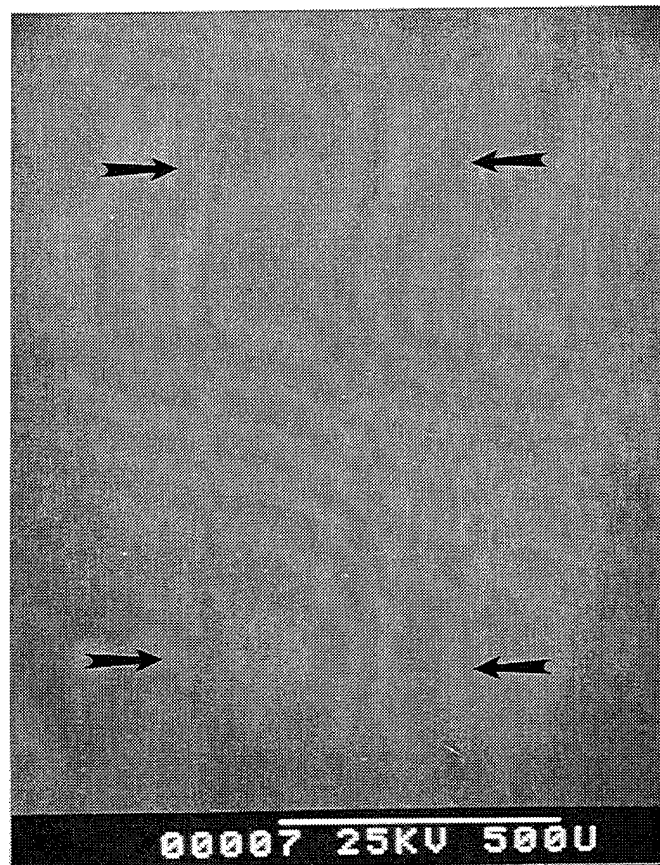
The RCF test data (see Figure 26) conclusively demonstrated that surface compression can increase the fatigue lifetime of SiC. SEM failure analysis showed a remarkable difference in the failure modes of the two CVD coatings. The CVD SiC/SiC failed due to microfracturing in the CVD SiC as shown in the left-hand micrograph of Figure 29. The right-hand photograph shows no wear, indicative of CVD SiC/SiC-30 vol. % TiC samples which did not fail ($\approx 70\%$ of those tested did not spall). Figure 30 confirms the reduced wear of the CVD SiC with $\approx -680\text{ MPa}$ residual stress. After 100 hours of testing (≈ 50 million cycles) there was no volume loss of the CVD SiC, whereas the brittle fracture of the CVD SiC under lower residual stress ($\approx -150\text{ MPa}$) showed volume loss due to its lower apparent toughness. SEM fractography showed that the spalls in the CVD SiC on SiC-30 vol. % TiC initiated very near the surface. Figure 31 shows a typical spall of the CVD SiC/SiC-30 vol. % TiC. The high surface compression caused catastrophic failure (see Figure 31(a)). Figures 31(b), 31(c) and 31(d) show successively higher magnification photographs of the failure origin. In Figure 31(d) it is evident that fracture initiated from SiC nodules formed in the CVD process. Figure 32 is an etched cross-section of the near surface region showing the pattern expected due to the nodular SiC growth which initiated failure.

It is hypothesized that there is a minimum apparent toughness needed to avoid the microfracturing that terminated the tests on the CVD SiC/SiC rods. SiC, SiC-10 vol. % TiC, SiC-20 vol. % TiC, SiC-30 vol. % TiC, and SiC-40 vol. % TiC rods were slip cast and sintered. They will be coated in the same CVD cycle, and RCF tested to determine the level of residual stress required to avoid "wear" caused by microfracture. This work will be continued as part of a Ph.D. thesis at the University of Utah under Professor Shetty's direction.

It is furthermore felt that if the CVD process can be improved to avoid the defects shown in Figure 33, as well as the nodule formation, then CVD SiC will work at 5.5 GPa in rolling contact fatigue testing. Discussions with Du Pont/Lanxide have indicated that coating in a fluidized bed would eliminate the nodule problem, as well speed up the coating process. A fluidized bed coating technique using CVD SiC on an inexpensive substrate should be investigated to see if the economics are attractive.



(a)



(b)

Figure 29. Comparison of wear tracks on (a) CVD SiC on SiC ($\sigma_R = -141$ MPa) after one million cycles and (b) CVD SiC on SiC-30 vol. % TiC ($\sigma_R = -679$ MPa) after 51.6 million cycles in rolling contact fatigue at 5.5 GPa. Note microfracturing when apparent toughness is low (a) and absence of microfracturing when compressive stresses are high (arrows in Fig. (b) denote location of wear track).

Three-Ball-on-Rod RCF Test

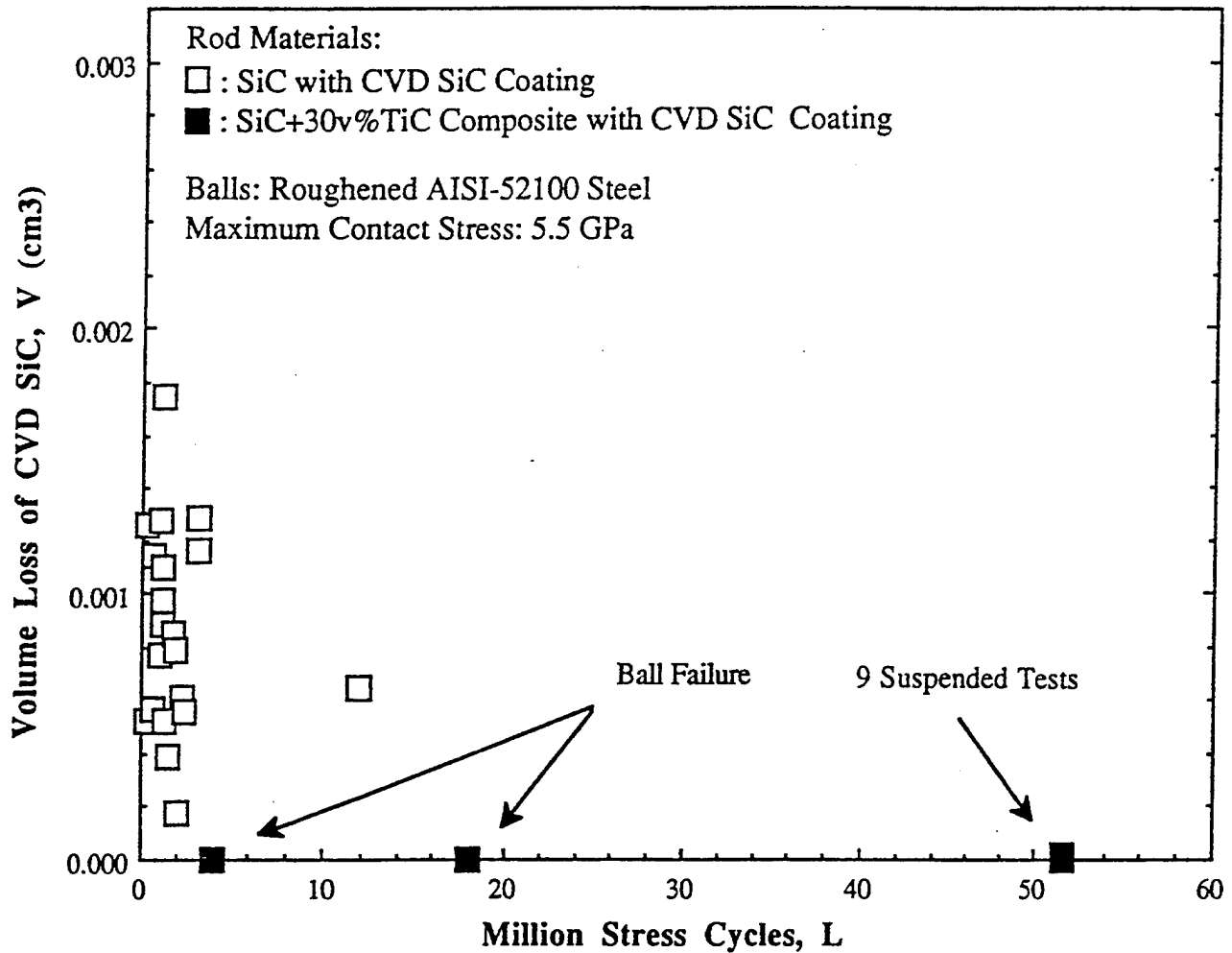
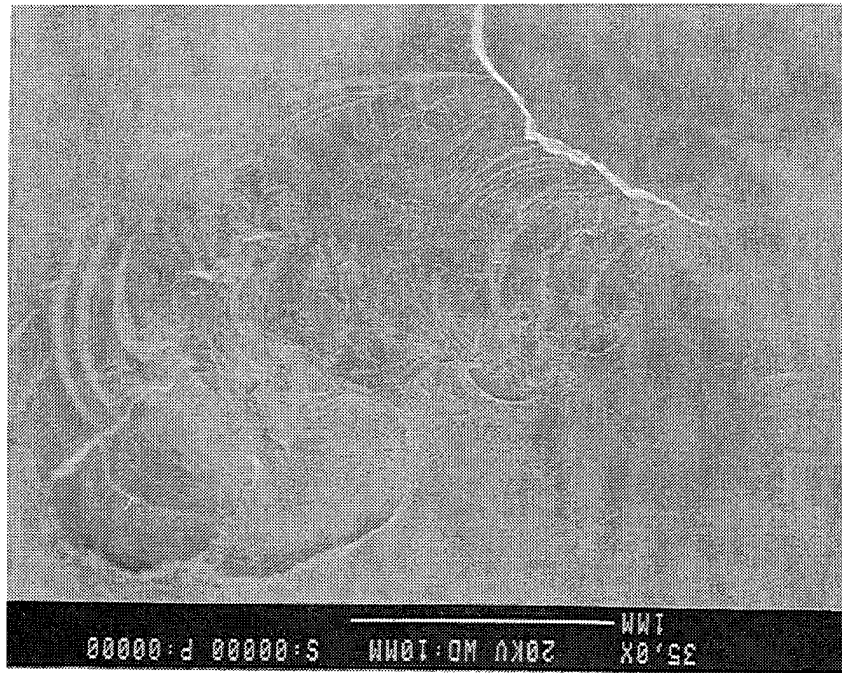
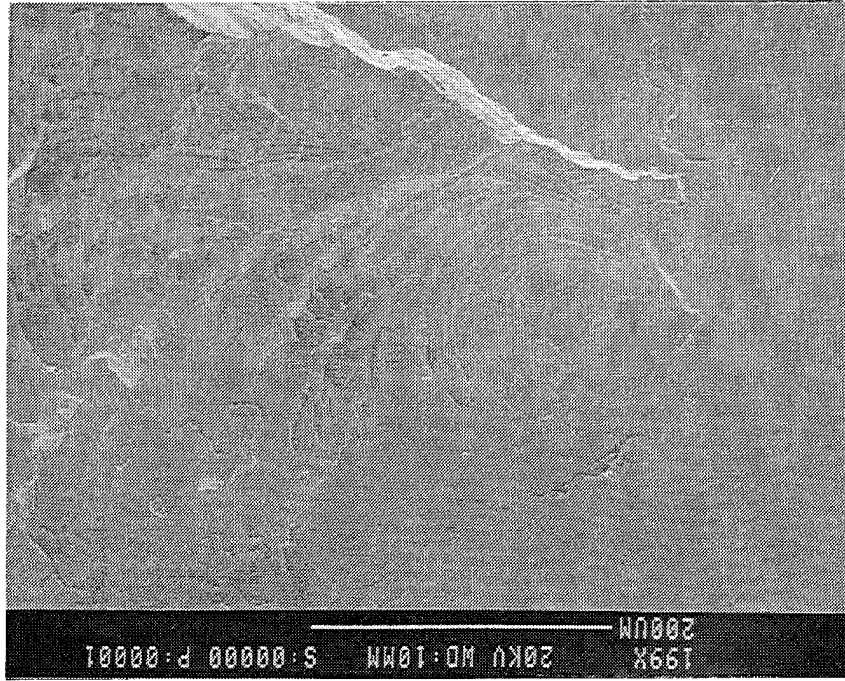


Figure 30. Volume loss as a function of RCF stress cycles. Note that "wear" is not measurable for CVD SiC on SiC-30 vol. % TiC due to higher apparent toughness compared to CVD SiC/SiC system.

Large-Scale Fracture Occurred on CVD SiC Coated SiC-30v%TiC



(a)

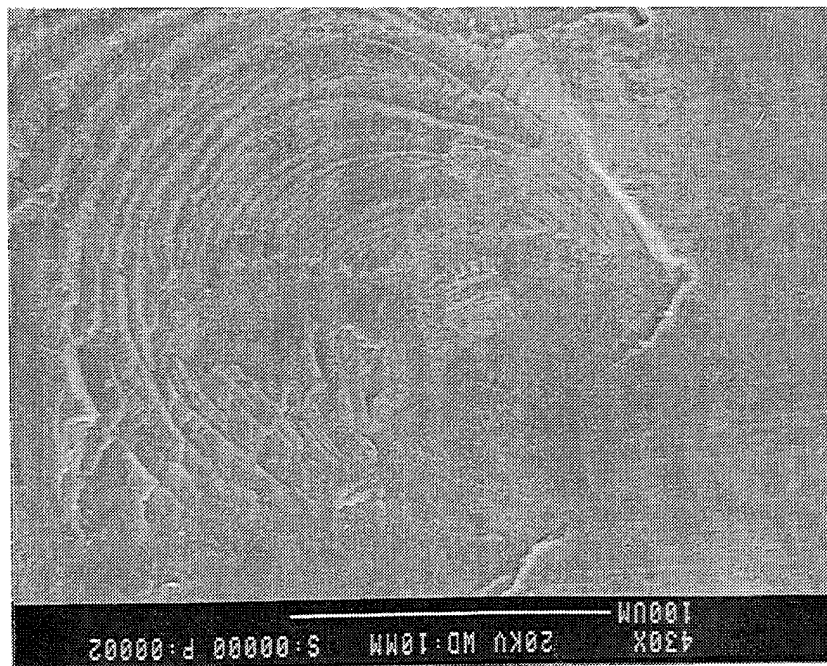


(b)

Rolling Direction



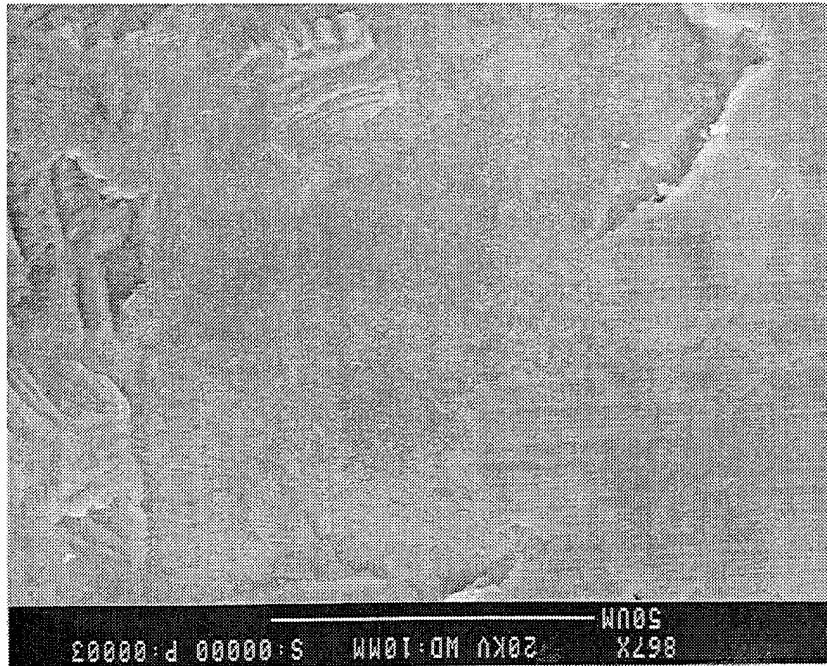
Figure 31. Fractography of failed CVD SiC/SiC-30 vol. % TiC.



(c)

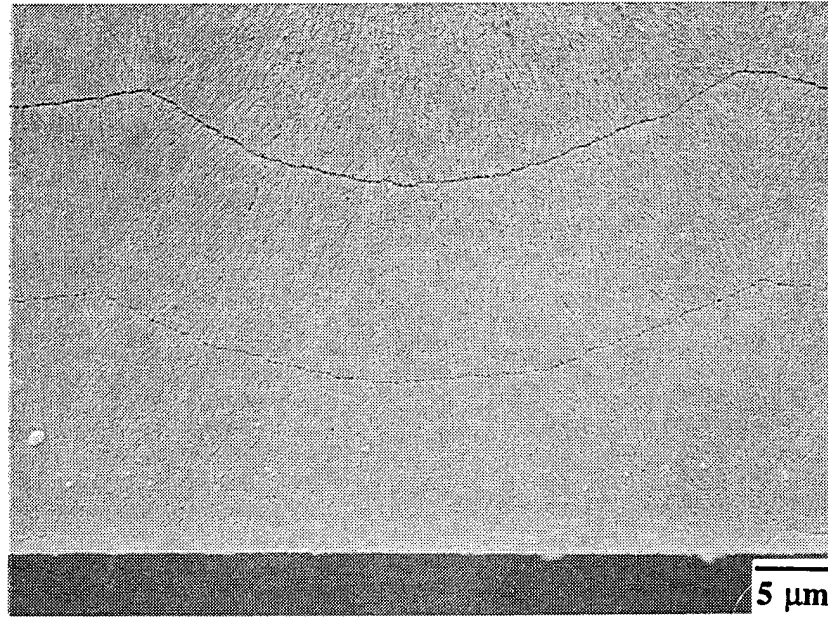


Rolling Direction

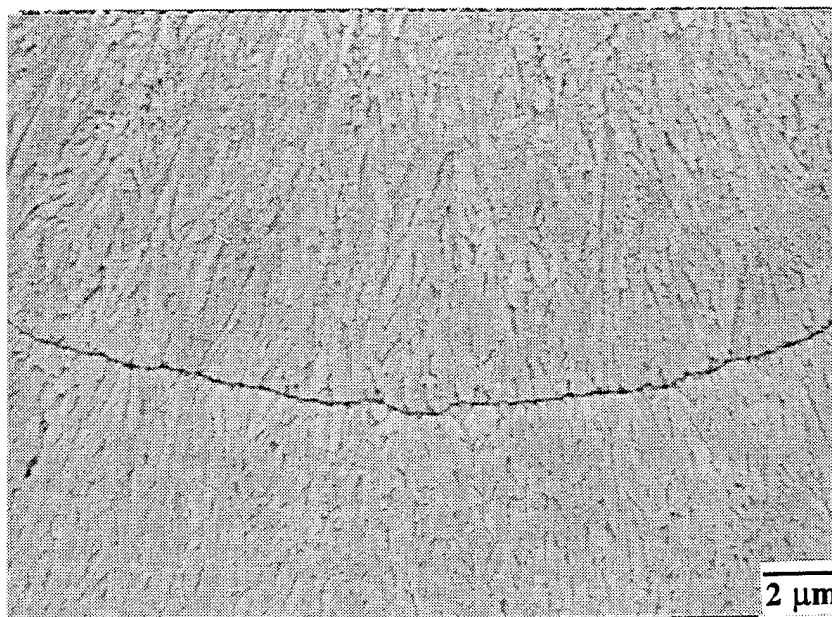


(d)

Figure 31 (continued).

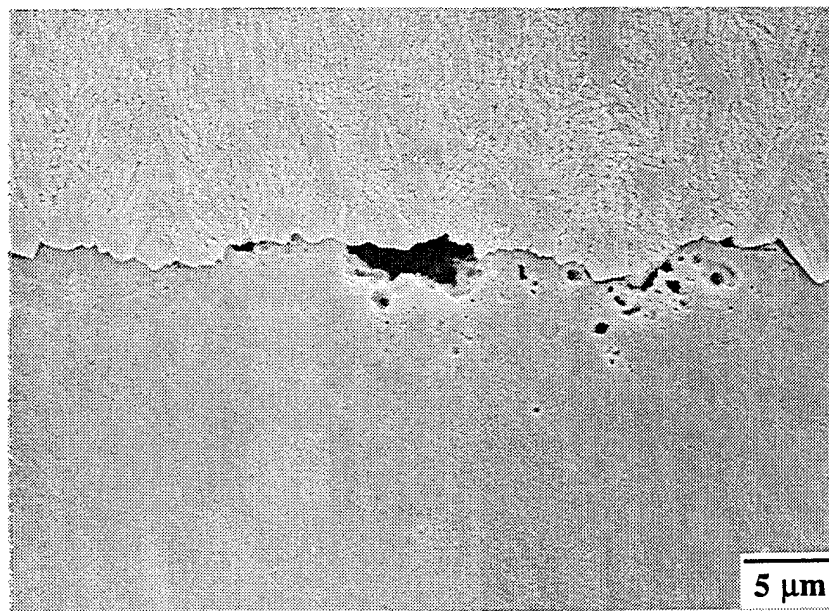


(a)

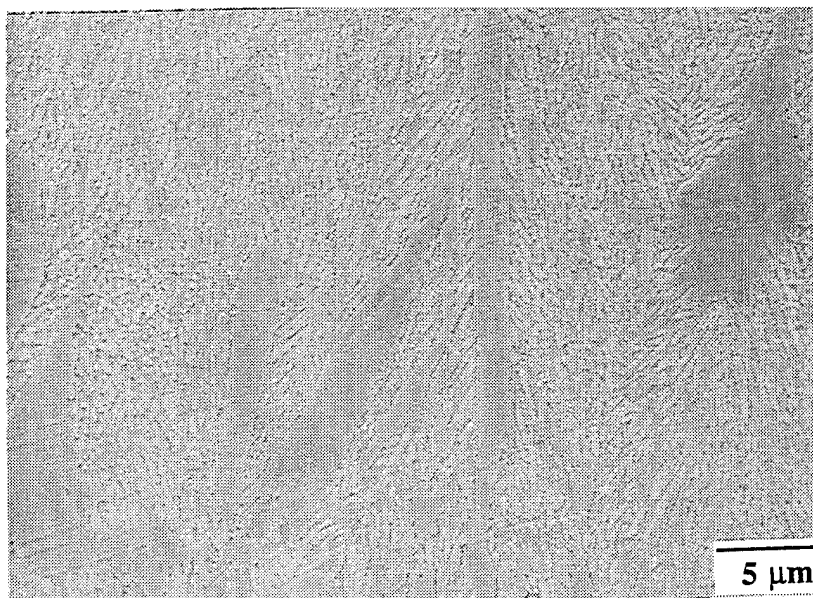


(b)

Figure 32. Near surface SEM micrographs of polished and etched CVD SiC/SiC-30 vol. % TiC showing SiC nodule growth in CVD process. (a) Layered substructure in CVD SiC coating, (b) interface between two layers in the CVD SiC coating.



(a)



(b)

Figure 33. SEM micrographs of polished and etched CVD SiC/SiC-30 vol. % TiC showing defects in CVD SiC. (a) An interface caused by process interruption, (b) large SiC grains (i.e., columnar growth of micrograin SiC) within the CVD SiC coating.

5. TECHNOLOGY TRANSFER/COMMERCIALIZATION PLANS

The possibility of CVD SiC coated ball bearings using an inexpensive substrate should be investigated. It is believed that if the modulus of a carbon/graphite material could be increased to ≈ 200 GPa by mixing in fine SiC to increase the modulus and controlling the thermal expansion with TiC additions, a C-SiC composite could be made in furnaces presently used to make graphite without substantially increasing the cost. Discussions with industry suggest that it should be possible to test this experimentally. If successful, near net shaped balls could be made spherical before inserting them into a fluidized bed. General Atomic has been contacted to assess the cost of fluidized bed CVD coating. Heart valves are commercially coated in a fluidized bed by suspending the valves in a bed of small balls. Using this same equipment (a 25 cm diameter reactor with a 200 cm³ working volume), it is estimated that $\approx 4,000$ 4 mm balls can be coated simultaneously at a cost of \$0.50/ball. This cost could be reduced by a factor of four if a reactor twice the diameter were used. These numbers are only estimates, but it appears that CVD SiC could substantially reduce the cost of ceramic bearings if an inexpensive substrate can be coated. Since graphite is already used in the semiconductor industry and can be coated well with CVD SiC if the thermal expansion mismatch is minimized, it would appear that a C-SiC may be a suitable inexpensive substrate when produced in large quantities.

While the SiC/C-SiC balls would be lighter than Si₃N₄, the only advantage currently of interest is cost. Lower cost is possible due to: a) low cost raw materials and large scale manufacturing typical of the graphite industry, b) elimination of the HIPing step, and c) the ease with which CVD SiC can be finished. There are many unknowns at the present time and experiments are necessary before a serious cost assessment can be made. In order to commercialize this technology the following steps should be taken:

- 1) Demonstrate with RCF rod testing that CVD SiC/SiC-TiC rods can be made to last 100 hours (20 out of 20 tests). This would involve testing monolithic SiC and SiC-TiC rods of controlled thermal expansion (i.e., SiC, SiC-10 vol. % TiC, SiC-20 vol. % TiC, SiC-30 vol. % TiC and SiC-40 vol. % TiC) by coating three rods of each composition simultaneously. It is suggested that three vendors be used to compare the CVD SiC deposited.

- 2) Demonstrate that CVD SiC/SiC-TiC balls can be coated in a fluidized bed and compare the ease of finishing these balls with Si₃N₄ balls finished at the same time. This would tell whether cost estimates for CVD coating are realistic and would show whether there is any cost saving in finishing operations.

3) Demonstrate that C-SiC can be fabricated economically by industry and that the thermal expansion can be controlled. Coat these rods and test as in step 1 above.

4) Demonstrate that CVD SiC/C-SiC balls can be coated and survive 100 hours at 5.5 GPa in RCF testing.

5) Promote the commercialization of this product by making any patent protection received readily available to companies willing to commercialize the technology.

6. CONCLUSIONS

Slip casting and cosintering was used on three different systems: 1) SiC-15 vol. % TiC/SiC-30 vol. % TiC, 2) Si₃N₄/Si₃N₄-15 vol. % TiN, and 3) Si₃N₄/Si₃N₄-20 vol. % TiN. Residual compressive stresses of 300-600 MPa were introduced using this approach. RCF testing showed that the layered ceramics have only marginally better performance as compared to the monolithic ceramics. Fractography suggested that structural defects (i.e., pores and agglomerates) are spall initiation sites in these materials. Improved processing steadily increased the fatigue lifetimes in these materials. RCF testing on the third set of materials (i.e., Si₃N₄/Si₃N₄-20 vol. % TiN) with improved density (>99.5 % of theoretical) showed no evidence of fatigue spalling. Cosintering can be used to make materials with high residual compression in the outer layers but HIPing is still required to eliminate processing flaws, resulting in no economical advantage to this approach.

CVD SiC, on the other hand, when deposited on SiC-30 vol. % TiC substrates, not only had high residual stress (\approx 680 MPa) but also showed extended fatigue lifetimes and reduced wear as compared to CVD SiC applied to a SiC substrate which resulted in low residual stress (\approx 140 MPa). CVD has the advantage that it can be used for making uniform layers on spherical rolling elements. The CVD approach was only limited by defects (i.e., nodular growth) in the SiC coating and the economics of coating. It is believed that both of these challenges can be overcome by using inexpensive substrates and a fluidized bed reactor.

The objectives of demonstrating increased RCF lifetimes and decreased wear rates have been met during this two year program. The third objective of demonstrating increased reliability should be a natural consequence of iterative testing and it is believed that this can be demonstrated by limiting nodule formation during CVD coating. It is strongly recommended that ARPA funding be continued in order to obtain the additional data (see above) needed so that commercialization can occur.

7. ACKNOWLEDGMENTS

Appreciation is expressed to Paul Gray of Du Pont Lanxide for helpful discussions and for coating bars and rods with CVD SiC at no cost to the program. Discussions with Prof. Anil V. Virkar of the University of Utah, Dr. Thomas Watkins of Oak Ridge National Laboratory, Dr. Godfried Basenbrook of General Atomic Corporation, and Doug Miller of Union Carbide Corporation are appreciated.

8. REFERENCES

1. A. V. Virkar, "Determination of Residual Stress Profile Using a Strain Gage Technique," *J. Am. Ceram. Soc.*, **73**[7] 2100-02 (1990).
2. D. Glover, "A Ball-Rod Rolling Contact Fatigue Tester," pp. 107-24 in *ASTM STP 771* ed. by J. J. C. Hoo (Am. Soc. Test. & Mater. 1982).
3. H. R. Baumgartner, "Ceramic Bearings for Turbine Applications," pp. 423-443 in *Ceramics for High Performance Applications-II*, ed. by J. J. Burke, E. N. Leno, and R. N. Katz (Brook Hill Publ. Co., Chestnut Hill, MA, 1978).
4. R. A. Cutler and T. B. Jackson, "Liquid Phase Sintered Silicon Carbide," pp. 309-18 in *Ceram. Mater. and Components for Engines*, ed. by V. J. Tennery (Am. Ceram. Soc., Westerville, OH 1989).
5. J. F. Chudecki, "Ceramic Bearings-Applications and Performance Advantages in Industrial Applications," SAE Technical Paper Series, Paper No. 891904 (1989).
6. E. V. Zaretsky and W. L. Anderson, "Rolling Contact Fatigue Studies With Four Tool Steels and a Crystallized Glass Ceramic," *Journal of Basic Engineering*, **83** [4] 603-612 (1961).
7. K. M. Taylor, L. B. Sibley and J. C. Lawrence, "Development of a Ceramic Rolling Contact Bearing for High Temperature Use," *Wear*, **6** [3] 226-40 (1963).
8. R. J. Parker, S. J. Grisaffe and E. V. Zaretsky, "Rolling-Contact Studies With Four Refractory Materials to 2000 F," *ASLE Transactions*, **8** [3] 208-16 (1965).
9. C. W. Dee, "Silicon Nitride-Tribological Applications of a Ceramic Material," *Tribology*, **3** [2] 89-92 (1970).
10. D. Scott, J. Blackwell and P. J. McCullagh, "Hot Pressed Silicon Nitride as a Rolling Bearing Material-A Preliminary Assessment," *Wear*, **17** [1] 73-82 (1971).
11. D. Scott and J. Blackwell, "Hot Pressed Silicon Nitride as a Rolling Bearing Material - A Preliminary Assessment," *Wear*, **24** [1] 61-67 (1973).
12. R. J. Parker and E. V. Zaretsky, "Fatigue Life of High-Speed Ball Bearings With Silicon Nitride Balls," *Journal of Lubrication Technology*, **97** [3] 350-57 (1975).
13. H. R. Baumgartner and W. M. Whieldon, "Rolling Contact Fatigue performance of Hot-Pressed Silicon Nitride Versus Surface preparation Techniques," pp. 179-93 in *Surfaces and Interfaces of Glasses and Ceramics*, V. D. Frechette, W. C. LaCourse and V. L. Burdick, eds., Plenum Press, New York (1973).
14. H. R. Baumgartner, "Evaluation of Roller Bearings Containing Hot Pressed Silicon Nitride Rolling Elements," pp. 713-27 in *Ceramics for High Performance Applications*, J. J. Burke, A. E. Gorum and R. N. Katz, eds., Brook Hill Publishing Co., Chestnut Hill, MA (1973).
15. R. N. Katz, "Ceramics for High Performance Rolling Element Bearings: A Review and Assessment," *Int. J. of High Technology Ceramics*, **1**, 69-79 (1985).
16. B. Bhushan and L. B. Sibley, "Silicon Nitride Rolling Bearings for Extreme Operating Conditions," *ASLE Transactions*, **25** [4] 417-28 (1982).
17. J. M. Reddecliff and R. Valori, "The Performance of a High-Speed Ball Thrust Bearing Using Silicon Nitride Balls," *Journal of Lubrication Technology*, **98** [4] 553-63 (1976).
18. J. R. Miner, W. A. Grace and R. Valori, "A Demonstration of High-Speed Gas Turbine Bearings Using Silicon Nitride Rolling Elements," *Lubrication Engineering*, **37** [8] 462-64, 473-78 (1981).
19. R. T. Cundill, "Material Selection and Quality For Ceramic Rolling Elements," pp. 905-12 in *Ceramic Materials and Components for Engines*, edited by R. Carlsson. Elsevier, London and New York (1992).
20. J. W. Lucek, "Rolling Wear of Silicon Nitride Bearing Materials," Paper # 90-GT-165, Presented at Gas Turbine and Aeroengine Congress and Exposition, June 11-14, Brussels (1990).

21. Y. Nishihara, H. Nakashima, N. Tsushima and S. Ito, "Factors That Affect Rolling Contact Fatigue Life of Ceramics and Rolling Contact Fatigue Life of Ceramic Balls and Rollers," Paper # 90-GT-377, presented at Gas Turbine and Aeroengine Congress and Exposition, June 11-14, Brussels (1990).
22. S. A. Horton, "Detection of Surface Defects in Ceramic Rolling Elements," pp. 897-904 in Ceramic Materials and Components for Engines. Edited by R. Carlsson. Elsevier, London and New York (1992).
23. F. J. Ebert, "Performance of Silicon Nitride (Si_3N_4) Components in Aerospace Bearing Applications," Paper # 90-GT-166, Presented at Gas Turbine and Aeroengine Congress and Exposition, June 11-14, Brussels (1990).
24. E. V. Zaretsky, "Ceramic Bearings for Use in Gas Turbine Engines," *J. of Gas Turbines and Power*, Trans. ASME, **111** [1] 146-57 (1989).
25. A. J. Gentile and A. D. Martin, "The Effect of Prior Metallurgically Induced Compressive Residual Stress on the Metallurgical and Endurance Properties of Overload Tested Ball Bearings," ASME Paper 65-WA/CF-7, American Society of Mechanical Engineers, Nov. (1965).
26. R. L. Scott, R. K. Kepple and M. H. Miller; pp. 301-16 in Rolling Contact Phenomena, J. B. Bidwell, Ed., Elsevier, North Holland, New York (1962)
27. A. V. Virkar, "Ceramic Bodies Having Plurality of Stress Zones," U. S. Pat. No. 4,656,071 (April 7, 1987).
28. A. V. Virkar, J. L. Huang and R. A. Cutler, "Strengthening of Oxide Ceramics by Transformation-Induced Stresses," *J. Am. Ceram. Soc.*, **70** [3] 164-70 (1987)
29. R. A. Cutler, J. D. Bright, A. V. Virkar and D. K. Shetty, "Strength Improvement in Transformation-Toughened Alumina by Selective Phase Transformation," *J. Am. Ceram. Soc.*, **70** [10] 714-18 (1987)
30. R. A. Cutler, J. J. Hansen, A. V. Virkar, D. K. Shetty and R. C. Winterton, "Strength Improvement in Transformation-Toughened Ceramics Using Compressive Residual Stresses," pp. 155-63 in Advanced Structural Ceramics, Volume 78. Edited by P. F. Becher, M. V. Swain and S. Somiya. Materials Research Society, Pittsburgh, PA, 1987.
31. J. J. Hansen, R. A. Cutler, D. K. Shetty and A. V. Virkar, "Indentation Fracture Response and Damage Resistance of Al_2O_3 - ZrO_2 Composites Strengthened by Transformation-Induced Residual Stresses," *J. Am. Ceram. Soc.*, **71** [12] C-501-C-505 (1988)
32. R. A. Cutler, C. B. Brinkpeter, A. V. Virkar and D. K. Shetty, "Fabrication and Characterization of Slip-Cast Layered Al_2O_3 - ZrO_2 Composites," pp. 397-408 in Ceramic Materials and Components for Engines. edited by R. Carlsson. Elsevier, London and New York (1992).
33. A. V. Virkar, J. F. Jue, J. J. Hansen and R. A. Cutler, "Measurement of Residual Stresses in Oxide- ZrO_2 Three-Layer Composites," *J. Am. Ceram. Soc.*, **71** [3] C-148-C-151 (1988).
34. A. K. Varshneya, "Stresses in Glass-to-Metal Seals," pp. 276-81 in Treatise on Materials Science and Technology, Vol. 22, Academic Press, Inc. (1982).
35. E. V. Zaretsky, "Selection of Rolling-Element Bearing Steels for Long-Life Applications," pp. 5-43 in Effect of Steel Manufacturing Processes on the Quality of Bearing Steels, ASTM STP 987, J. J. C. Hoo, Ed., American Society for Testing and Materials, Philadelphia (1988)
36. T. B. Jackson, A. C. Hurford, S. L. Bruner and R. A. Cutler, "SiC-Based Ceramics with Improved Strength," pp. 227-40 in SiC '87, ed. by J. D. Cawley and C. E. Semler, Am. Ceram. Soc., Westerville, OH (1988).
37. R. A. Cutler, A. V. Virkar and A. C. Hurford, "Liquid-Phase Sintering of Silicon Carbide," U. S. Patent 4,829,027 (1989)
38. S. Gochnour, J. D. Bright, D. K. Shetty and R. A. Cutler, "Solid Particle Erosion of SiC- Al_2O_3 Ceramics", *J. Mater. Sci.*, 3229-35 (1990).

39. K. Y. Chia and S. K. Lau, "High Toughness Silicon Carbide," *Ceram. Sci. and Eng. Proc.* **10**[7-8] (1991).
40. M. L. Torti and D. W. Richerson, "High Strength Composite Ceramic Structure," U. S. Patent 3,911,188 (Oct. 7, 1975).
41. J. J. Stiglich and D. G. Bhat, "Friction and Erosive Wear of Controlled Nucleation Thermochemically Deposited W-C Alloys and SiC and Chemically Vapor-Deposited Si_3N_4 ," *Thin Solid Films*, **72**, 503-9 (1980).
42. M. J. Listen, private communication with D. K. Shetty (1991).
43. W. Boecker, R. S. Storm, and K Y Chia, "Silicon Carbide Bodies Having High Toughness and Fracture Resistance and Method of Making Same," *Eur. Pat. Appl.* 419 271 A2 (March 27, 1991).
44. W. Boecker and R. Hamminger, "Advancements in Sintering of Covalent High-Performance Ceramics," *Interceram*, **40**[7] 520-25(1991).
45. E. M. Levin, C. R. Robbins, and H. F. McMurdie, Phase Diagrams for Ceramists, 1969 Supplement, Figure 2586 (Am. Ceram. Soc., Westerville, OH, 1969).
46. E. Kamijo, M. Honda, M. Higuchi, H. Takeuchi, and T. Tanimura, "Processing of Electroconductive Ceramic Composites," *Sumitomo Electr. Tech. Rev.*, **24**, 183-92 (1985).
47. C. Martin, B. Cales, P. Vivier, and P. Mathieu, "Electrical Discharge Machinable Ceramic Composites," *J. Mater. Sci. & Eng.*, **A109**, 351-56 (1989).
48. Y. Yasutomi and M. Sobue, "Development of Reaction-Bonded Electroconductive $\text{TiN-Si}_3\text{N}_4$ and Resistive $\text{Al}_2\text{O}_3\text{-Si}_3\text{N}_4$ Composites," *Ceram. Eng. Sci. Proc.*, **11**[7-8] 857-67 (1990).
49. Engineering Property Data on Selected Ceramics, Vol. I, Nitrides, Battelle Columbus Laboratories Report MCIC-HB-07 (Battelle Columbus Laboratories Metals and Ceramics Information Center, Columbus, OH 1976).
50. G. C. Wei and P. F. Becher, "Improvements in Mechanical Properties in SiC by the Addition of TiC Particles," *J. Am. Ceram. Soc.*, **67**[8] 571-74 (1984).
51. Engineering Property Data on Selected Ceramics, Vol. II, Carbides, Battelle Columbus Laboratories Report MCIC-HB-07 (Battelle Columbus Laboratories Metals and Ceramics Information Center, Columbus, OH 1979).
52. M. Schwelm, G. Kaiser, W. Schulz, H. Schubert and G. Petzow, "The Effect of Alcohol Treatment on the Rheology of Si_3N_4 ," *J. Europ. Ceram. Soc.*, **11**, 283-89 (1993).
53. T. R. Watkins and D. J. Green, "Fracture Behavior of Chemically-Vapor-Deposited SiC-Coated Graphite: I, Experimental Results," *J. Am. Ceram. Soc.*, **76**[12] 3066-72 (1993).